Design, synthesis, antiproliferative activity, and molecular dynamics simulation of pyrazoline-based derivatives as dual EGFR and HER-2 inhibitors†

Hani Mohamed Hafez, [ID] [a] Basmat Amal M. Said,[b] Ahmed M. Sayed,[cd] Eid Alatwi,[e] Bahaa G. M. Youssif [ID] *[f] Stefan Bräse [ID] *[g] and Hany A. M. El-Sherief [ID] [h]

The dual targeting of EGFR and HER2 is an established anticancer strategy. A novel series including two distinct scaffolds, A (chalcone-based compounds, **4a–n**) and B (pyrazoline-based compounds, **5a–n**), was developed and synthesized. The antiproliferative efficacy of **4a–n** and **5a–n** was examined against a panel of four cancer cell lines. The findings indicated that pyrazoline derivatives **5a–n** exhibited more efficacy than chalcone compounds **4a–n**. Compounds **4n**, **5d**, and **5g** were identified as the most effective antiproliferative derivatives. These compounds were further investigated as dual EGFR/Her2 inhibitors. Compound **5d** inhibited EGFR-TK and HER2 significantly, with IC_{50} values of 0.126 and 0.061 μM, respectively. Moreover, compound **5d** can induce a percentage of pre-G1 apoptosis by 78.53% in cell cycle analysis and cause early apoptosis with necrosis percent of 5.28. Docking and MD simulation illustrated the significant cytotoxic activity of the **5d** compound and how it can be a promising scaffold with anticancer activity.

1. Introduction

Receptor tyrosine kinases (RTKs) are a class of tyrosine kinases that help transfer a phosphate group from ATP to a hydroxyl group on a tyrosine residue. These enzymes regulate various tasks in normal cells, including growth, motility, differentiation, and metabolism. Furthermore, they are crucial to oncogenesis.[1,2] There are 58 known receptor tyrosine kinases (RTKs) in humans, which are divided into 20 subfamilies. These include the ERBB receptors, the insulin receptors, the platelet-

[a]Pharmaceutical Chemistry Branch, College of Pharmacy, Al-Esraa University College, Baghdad, Iraq

[b]College of Pharmacy, Al-Mustaqbal University, Babylon, 51001, Iraq

[c]Department of Pharmacognosy, Faculty of Pharmacy, Nahda University, 62513 Beni Suef, Egypt

[d]Department of Pharmacognosy, Collage of Pharmacy, Almaaqal University, 61014 Basrah, Iraq

[e]Department of Pharmacology, College of Pharmacy, Jouf University, Sakaka 72341, Aljouf, Saudi Arabia

[f]Department of Pharmaceutical Organic Chemistry, Faculty of Pharmacy, Assiut University, Assiut 71526, Egypt. E-mail: bgyoussif2@gmail.com; Tel: +20-1098294419

[g]Institute of Biological and Chemical Systems-Functional Molecular Systems (IBCS-FMS), Karlsruhe Institute of Technology, 76131 Karlsruhe, Germany. E-mail: braese@kit.edu

[h]Department of Pharmaceutical Chemistry, Faculty of Pharmacy, Deraya University, Minia, Egypt

† Electronic supplementary information (ESI) available. See DOI: https://doi.org/10.1039/d5ra01169h

derived growth factor (PDGF) receptors, and the vascular endothelial growth factor (VEGF) receptors.[3,4] ERBB, a subclass I of the receptor tyrosine kinase superfamily, comprises four members: EGFR/ERBB1/HER1, ERBB2/HER2, ERBB3/HER3, and ERBB4/HER4. These members have a similar protein structure, with a tyrosine kinase-containing cytoplasmic domain, an extracellular ligand-binding domain, and a single transmembrane helix.[5] According to reports, the epidermal growth factor receptor (EGFR) plays a crucial role in tumor growth and progression, including cell proliferation, apoptosis inhibition, metastasis, and angiogenesis.[6,7] Moreover, HER2 functions as a significant cancer biomarker despite the absence of a ligand for it. HER2 must dimerize to be activated, and heterodimers formed between HER2, and other ERBB family members have gotten much attention because they are more stable and send signals more effectively. Oncological treatment, considered a significant target, typically generates EGFR/HER2 heterodimers.[8]

Pyrazolines are five-membered heterocycles that consist of two adjacent nitrogen atoms and an endocyclic double bond in the ring structure. Of the three tautomeric structures of pyrazolines, 2-pyrazoline is the most prevalent.[9] Researches reveal that diversely substituted pyrazolines exhibit various pharmacological actions, including anticancer effects. Certain pyrazoline-derived cytotoxic agents exhibit cancer chemopreventive characteristics.[10–13]
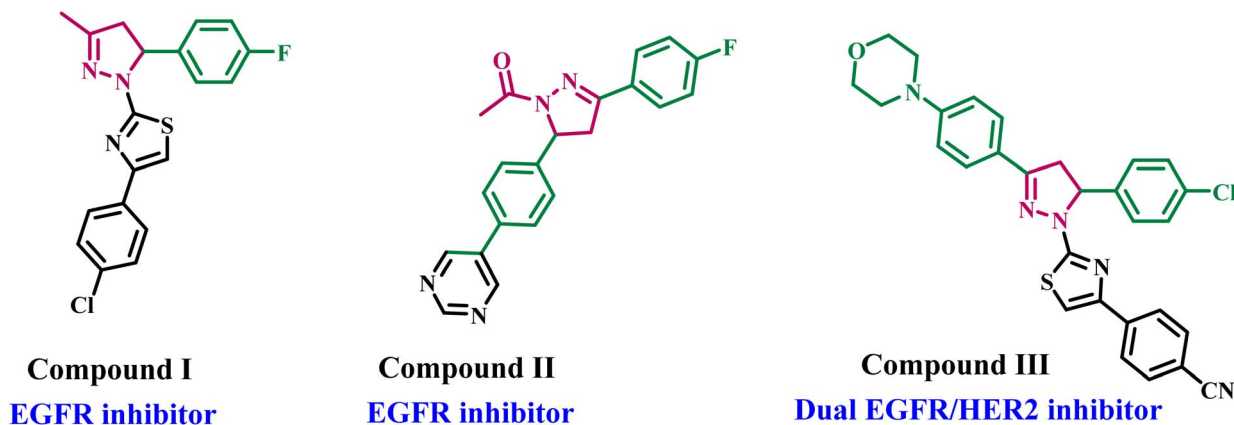
Paper

Fig. 1 Structures of some pyrazoline-based derivatives as EGFR and/or HER2 inhibitors I–III.

For example, Lv and colleagues demonstrated that the pyrazoline-based derivative **I** (Fig. 1) exhibited significant cytotoxicity against the breast cancer cell line (MCF-7), with an IC_{50} of 0.07 μM, through EGFR inhibition, which had an IC_{50} value of 0.06 μM.[14] Al-Anazi et al.[15] developed a novel series of pyrazoline-based compounds as EGFR inhibitors. The cytotoxic effects of these compounds were examined on hormonal and non-hormonal breast cancer cell lines. Most pyrazoline derivatives have shown significant cytotoxic effects against hormonal breast cancer. In vitro tests have shown compound **II** (Fig. 1) is the most potent pyrazoline derivative, blocking the EGFR kinase at a very low concentration of 0.19 μM.

New pyrazoline derivatives were developed and evaluated for their cytotoxic activities against various cancer cell lines.[16] The results indicated compound **III** (Fig. 1) is the most potent derivative. Compound **III** caused apoptosis and had a strong EGFR inhibitory effect, with an IC_{50} of 4.34 μM compared to erlotinib's IC_{50} of 0.05 μM. Compound **III** significantly suppressed HER2, with an IC_{50} value of 2.30 μM, so it functions as a dual EGFR and HER2 inhibitor.

On the other hand, chalcones are aromatic ketones that serve as the fundamental structure for numerous essential biological molecules.[17] They exhibit diverse therapeutic properties and can be adaptable precursors for numerous complex compounds in medicinal chemistry.[18] Recent research indicates that chalcones demonstrate diverse biological activities, with the most prominent anticancer properties.[19,20] They may also reduce resistance to multiple chemotherapeutic agents.[21] Chalcones selectively limit cancer formation and progression, indicating that they and their derivatives may serve as viable options for cancer treatment.[22,23] Consequently, researchers are synthesizing various chalcones to assess their effectiveness in multiple therapeutic domains.

In a recent publication from our lab,[19] we describe a new series of quinoline/chalcone hybrids that work as antiproliferative agents and block both EGFR and $BRAF^{V600E}$. With an IC_{50} of 3.60 ± 0.60 μM for the MCF-7 breast cancer cell line, compound **IV** (Fig. 2) had the strongest antiproliferative effect against cancer cell proliferation of all the new hybrids. Furthermore, it demonstrated substantial inhibitory activity against EGFR and $BRAF^{V600E}$, with IC_{50} values of 2.30 and 4.60 μM, respectively.

In another publication,[24] we describe a novel series of quinoline/chalcone-based compounds that stop cell growth by targeting EGFR and $BRAF^{V600E}$. Compound **V** (Fig. 2) exhibited enhanced antiproliferative efficacy relative to doxorubicin (GI_{50} = 1.15 μM). It demonstrated a GI_{50} value of 3.30 μM against four human cancer cell lines. The compound showed significant
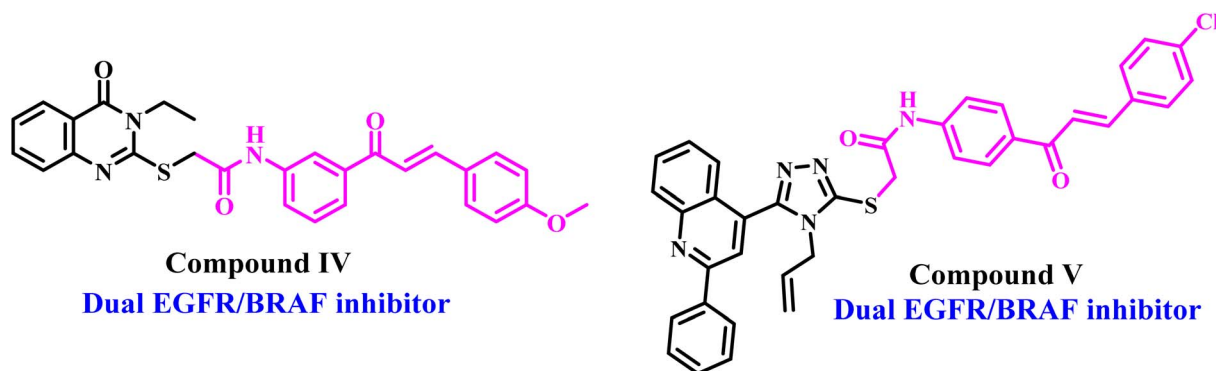

Fig. 2 Compounds IV and V as dual-targeting chalcone-based antiproliferative agents.
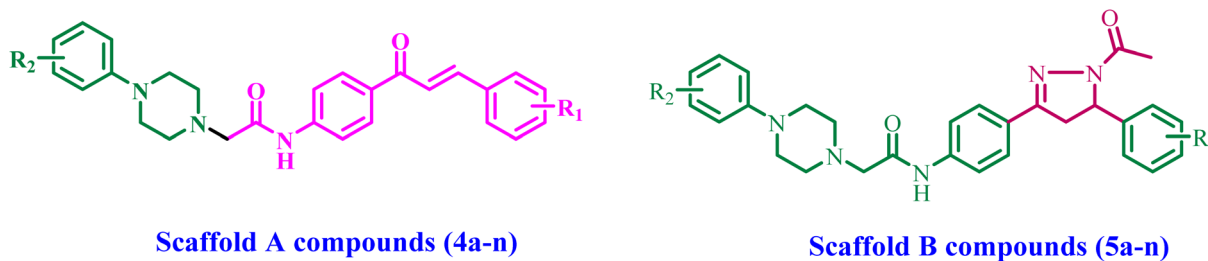
Fig. 3 Structures of new targets **4a–n** and **5a–n**.

inhibitory activity against EGFR and BRAF^{V600E}, with IC$_{50}$ values of 1.30 ± 0.12 µM and 3.80 ± 0.15 µM, respectively. In contrast, the reference erlotinib exhibited IC$_{50}$ values of 0.08 ± 0.005 µM for EGFR and 0.06 ± 0.01 µM for BRAF^{V600E}.

Building upon previously reported data and as part of our ongoing effort to develop a dual- or multi-targeted anti-proliferative agent,[12,13,25–28] this work details the development, synthesis, and biological evaluation of novel dual inhibitors aimed at EGFR and HER-2. The newly developed compounds are made up of two distinct scaffolds. Fig. 3 indicates that the scaffold A compounds (**4a–n**) are chalcone-based derivatives. The compounds in scaffold B are pyrazoline derivatives known as **5a–n** (Fig. 3). The newly synthesized compounds **4a–n** and **5a–n** will be tested against a panel of four cancer cell lines for antiproliferative activity. The most promising compounds will be further tested as dual EGFR/HER2 inhibitors. Furthermore, we will study the apoptotic potential of the most potent compound. Finally, we will use molecular docking and dynamic simulations to investigate these compounds' probable binding mechanisms and interactions with receptor sites.

2. Experimental

2.1. Chemistry

General details: see ESI Appendix A.†

2.1.1. General procedure for synthesis of *N*-(4-cinnamoyl-substituted-phenyl)-2-(4-substituted-phenylpiperazin-1-yl) acetamides (4a–n). An equimolar mixture of substituted phenylpiperazines hydrochloride **3a–b** and compound **2a–g** (0.01 mol) in DMF (5 mL) and K$_2$CO$_3$ (0.02 mol) was stirred for 24 h. The reaction mixture was poured onto ice, and the precipitate was filtered and recrystallized from ethanol, affording the chalcone derivatives, **4a–n**.

2.1.1.1. N-(4-Cinnamoylphenyl)-2-(4-(4-methoxyphenyl) piperazin-1-yl)acetamide (4a). Yellow powder (70% yield, 0.32 g), mp 163–165 °C. ^{1}H NMR (400 MHz, DMSO-d_6) δ 10.16 (s, 1H), 8.17 (d, $J = 8.2$ Hz, 2H), 7.95 (d, $J = 15.6$ Hz, 1H), 7.91–7.83 (m, 4H), 7.73 (d, $J = 15.6$ Hz, 1H), 7.52–7.40 (m, 3H), 6.89 (d, $J = 8.9$ Hz, 2H), 6.81 (d, $J = 8.8$ Hz, 2H), 3.67 (s, 3H), 3.36 (s, 2H), 3.08 (t, $J = 4.8$ Hz, 4H), 2.68 (t, $J = 4.9$ Hz, 4H); ^{13}C NMR (101 MHz, DMSO) δ 187.56, 168.91, 152.89, 145.37, 143.51, 143.40, 143.10, 142.90, 134.77, 132.81, 132.44, 130.59, 130.49, 129.96, 129.84, 128.90, 128.81, 121.97, 118.94, 118.81, 117.38, 114.23, 61.75, 55.15, 52.79, 49.46. Anal. calcd for C$_{28}$H$_{29}$N$_3$O$_3$ (455.56): C, 73.82; H, 6.42; N, 9.22 found: C, 73.91; H, 6.58; N, 9.46.

2.1.1.2. 2-(4-(4-Methoxyphenyl)piperazin-1-yl)-N-(4-(3-(p-tolyl) acryloyl)phenyl)acetamide (4b). Yellow powder (82% yield, 0.38 g), mp 158–160 °C. ^{1}H NMR (400 MHz, DMSO-d_6) δ 10.17 (s, 1H), 8.15 (d, $J = 8$ Hz, 2H), 8.00–7.62 (m, 6H), 7.25 (d, $J = 8$ Hz, 2H), 6.88 (d, $J = 8.8$ Hz, 2H), 6.80 (d, $J = 8.8$ Hz, 2H), 3.66 (s, 3H), 3.36 (s, 2H), 3.08 (t, $J = 4.8$ Hz, 4H), 2.68 (t, $J = 4.9$ Hz, 4H). 2.33 (s, 3H); ^{13}C NMR (101 MHz, DMSO) δ 187.56, 187.53, 168.94, 152.89, 145.38, 143.47, 143.43, 143.05, 142.99, 140.54, 132.67, 132.55, 132.07, 129.89, 129.76, 129.71, 129.53, 128.85, 120.92, 120.89, 118.93, 118.81, 118.66, 118.15, 117.38, 114.23, 62.06, 61.76, 55.14, 52.80, 49.48, 21.08. Anal. calcd for C$_{29}$H$_{31}$N$_3$O$_3$ (469.59): C, 74.18; H, 6.65; N, 8.95 found: C, 73.89; H, 6.79; N, 9.21.

2.1.1.3. N-(4-(3-(4-Methoxyphenyl)acryloyl)phenyl)-2-(4-(4-methoxyphenyl)piperazin-1-yl)acetamide (4c). Yellow powder (73% yield, 0.35 g), mp 123–125 °C. ^{1}H NMR (400 MHz, DMSO-d_6) δ 10.14 (s, 1H), 8.13 (d, $J = 12$ Hz, 2H), 7.89–7.82 (m, 3H), 7.78 (d, $J = 12$ Hz, 2H), 7.70 (d, $J = 15.5$ Hz, 1H), 7.01 (d, $J = 12$ Hz, 2H), 6.88 (d, $J = 9.2$ Hz, 2H), 6.81 (d, $J = 9.2$ Hz, 2H), 3.82 (s, 3H), 3.67 (s, 3H), 3.25 (s, 2H), 3.08 (t, $J = 6.5$ Hz, 4H), 2.68 (t, $J = 5.0$ Hz, 4H); ^{13}C NMR (101 MHz, DMSO) δ 187.46, 187.43, 168.91, 161.28, 152.89, 145.39, 143.51, 143.39, 143.35, 142.90, 142.82, 142.69, 133.10, 132.72, 130.71, 129.81, 129.68, 129.62, 127.43, 127.40, 119.45, 118.91, 118.78, 118.74, 117.39, 114.40, 114.24, 62.01, 61.77, 55.37, 55.16, 52.81, 49.48. Anal. calcd for C$_{29}$H$_{31}$N$_3$O$_4$ (485.58): C, 71.73; H, 6.44; N, 8.65 found: C, 71.95; H, 6.63; N, 8.84.

2.1.1.4. 2-(4-(4-Methoxyphenyl)piperazin-1-yl)-N-(4-(3-(3,4,5-trimethoxyphenyl)acryloyl)phenyl)acetamide (4d). Yellow powder (80% yield, 0.43 g), mp 162–164 °C. ^{1}H NMR (400 MHz, DMSO-d_6) δ 10.15 (s, 1H), 8.17 (d, $J = 8.7$ Hz, 2H), 7.91–7.83 (m, 3H), 7.66 (d, $J = 15.6$ Hz, 1H), 7.23 (s, 2H), 6.89 (d, $J = 9.1$ Hz, 2H), 6.81 (d, $J = 9.1$ Hz, 2H), 3.87 (s, 6H), 3.72 (s, 3H), 3.68 (s, 3H), 3.25 (s, 2H), 3.09 (q, $J = 4.9$ Hz, 4H), 2.67 (t, $J = 4.9$ Hz, 4H); ^{13}C NMR (101 MHz, DMSO) δ 187.50, 168.94, 153.11, 152.90, 145.39, 143.94, 143.06, 139.67, 132.55, 130.34, 129.83, 121.12, 118.77, 117.39, 114.24, 106.49, 61.80, 60.14, 55.16, 52.81, 49.48. Anal. calcd for C$_{31}$H$_{35}$N$_3$O$_6$ (545.64): C, 68.24; H, 6.47; N, 7.70 found: C, 68.40; H, 6.55; N, 7.89.

2.1.1.5. N-(4-(3-(4-Bromophenyl)acryloyl)phenyl)-2-(4-(4-methoxyphenyl)piperazin-1-yl)acetamide (4e). Yellow powder (81% yield, 0.43 g), mp 193–195 °C. ^{1}H NMR (400 MHz, DMSO-d_6) δ 9.50 (s, 1H), 8.05 (d, $J = 8.4$ Hz, 1H), 7.78–7.74 (m, 4H), 7.59–7.52 (m, 6H), 6.96 (d, $J = 8$ Hz, 2H), 6.88 (d, $J = 8$ Hz, 2H), 3.81 (s, 3H), 3.31 (s, 2H), 3.22 (t, $J = 4.8$ Hz, 4H), 2.88 (t, $J =$

4.9 Hz, 4H); ^{13}C NMR (101 MHz, DMSO-d_6) δ 187.42, 168.96, 152.89, 145.38, 143.18, 142.01, 134.10, 132.32, 131.86, 130.73, 129.89, 123.83, 122.77, 118.79, 117.39, 114.24, 61.78, 55.17, 52.80, 49.47. Anal. calcd for $C_{28}H_{28}BrN_3O_3$ (534.45): C, 62.93; H, 5.28; N, 7.86 found: C, 63.15; H, 5.47; N, 8.05.

2.1.1.6. N-(4-(3-(2,4-Dichlorophenyl)acryloyl)phenyl)-2-(4-(4-methoxyphenyl)piperazin-1-yl)acetamide (4f). Yellow powder (74% yield, 0.38 g), mp 142–145 °C. ^{1}H NMR (400 MHz, DMSO-d_6) δ 10.60 (s, 1H), 8.25 (d, J = 15.6 Hz, 1H), 8.16 (d, J = 8.5 Hz, 2H), 8.06–7.92 (m, 2H), 7.87 (d, J = 8.5 Hz, 2H), 7.77–7.75 (m, 1H), 7.55 (d, J = 15.6 Hz, 1H), 6.89 (d, J = 9.1 Hz, 2H), 6.81 (d, J = 9.0 Hz, 2H), 3.68 (s, 3H), 3.25 (s, 2H), 3.08 (t, J = 4.9 Hz, 4H), 2.68 (t, J = 4.9 Hz, 4H); ^{13}C NMR (101 MHz, DMSO) δ 187.17, 169.01, 152.89, 145.39, 143.42, 136.68, 136.64, 135.49, 135.08, 132.01, 131.48, 130.16, 130.04, 129.98, 129.81, 129.48, 129.41, 127.93, 127.83, 125.29, 118.94, 118.81, 118.67, 118.16, 117.39, 114.24, 61.75, 55.17, 52.79, 49.48. Anal. calcd for $C_{28}H_{27}Cl_2N_3O_3$ (524.44): C, 64.13; H, 5.19; N, 8.01 found: C, 64.39; H, 5.33; N, 8.29.

2.1.1.7. N-(4-(3-(Furan-2-yl)acryloyl)phenyl)-2-(4-(4-methoxyphenyl)piperazin-1-yl)acetamide (4g). Yellow powder (69% yield, 0.31 g), mp 187–189 °C. ^{1}H NMR (400 MHz, DMSO-d_6) δ 10.16 (s, 1H), 8.10–8.02 (m, 2H), 7.94–7.88 (m, 2H), 7.88–7.82 (m, 2H), 7.55–7.54 (m, 2H), 7.09–7.08 (m, 1H), 6.89 (d, J = 9.2 Hz, 2H), 6.81 (d, J = 9.2 Hz, 2H), 6.69 (m, 1H), 3.68 (s, 3H), 3.24 (s, 2H), 3.07 (d, J = 5.6 Hz, 3H), 2.67 (t, J = 4.9 Hz, 3H); ^{13}C NMR (101 MHz, DMSO) δ 187.04, 186.99, 168.94, 152.89, 151.23, 146.06, 145.39, 143.05, 143.00, 132.36, 129.96, 129.94, 129.59, 129.53, 119.00, 118.87, 118.70, 118.66, 117.39, 116.76, 116.71, 114.23, 113.09, 62.04, 61.75, 55.16, 52.79, 49.57, 49.48. Anal. calcd for $C_{26}H_{27}N_3O_4$ (445.52): C, 70.09; H, 6.11; N, 9.43 found: C, 70.25; H, 6.29; N, 9.64.

2.1.1.8. 2-(4-(4-Chlorophenyl)piperazin-1-yl)-N-(4-cinnamoyl-phenyl)acetamide (4h). Yellow powder (76% yield, 0.35 g), mp 188–190 °C. ^{1}H NMR (400 MHz, DMSO-d_6) δ 10.16 (s, 1H), 8.17 (d, J = 8.4 Hz, 1H), 7.96 (d, J = 15.7 Hz, 1H), 7.88 (t, J = 6.5 Hz, 2H), 7.74 (d, J = 15.6 Hz, 1H), 7.49–7.44 (m, 1H), 7.24 (d, J = 8.3 Hz, 1H), 6.96 (d, J = 8.8 Hz, 1H), 3.35 (s, 1H), 3.21 (d, J = 5.3 Hz, 2H), 2.69 (t, J = 4.9 Hz, 2H); ^{13}C NMR (101 MHz, DMSO) δ 187.55, 168.90, 149.79, 143.40, 143.32, 143.22, 143.11, 134.77, 132.43, 132.35, 130.50, 129.83, 129.76, 128.90, 128.81, 128.60, 61.63, 52.47, 47.91. Anal. calcd for $C_{27}H_{26}ClN_3O_2$ (459.97): C, 70.50; H, 5.70; N, 9.14 found: C, 70.63; H, 5.81; N, 9.39.

2.1.1.9. 2-(4-(4-Chlorophenyl)piperazin-1-yl)-N-(4-(3-(p-tolyl)acryloyl)phenyl)acetamide (4i). Yellow powder (70% yield, 0.33 g), mp 175–177 °C. ^{1}H NMR (400 MHz, DMSO-d_6) δ 10.12 (s, 1H), 8.15 (d, J = 8.2 Hz, 1H), 7.95–7.83 (m, 2H), 7.80–7.66 (m, 2H), 7.24 (dd, J = 19.3, 8.2 Hz, 3H), 6.94 (d, J = 8.7 Hz, 1H), 3.28–3.15 (m, 3H), 2.67 (t, J = 5.0 Hz, 2H), 2.35 (s, 2H); ^{13}C NMR (101 MHz, DMSO) δ 187.57, 187.53, 168.89, 149.80, 143.48, 143.44, 143.02, 142.96, 140.56, 140.55, 132.56, 132.07, 129.90, 129.77, 129.71, 129.54, 128.86, 128.70, 128.61, 122.31, 120.92, 120.89, 118.94, 118.82, 117.42, 116.85, 61.64, 52.48, 47.91, 21.09. Anal. calcd for $C_{28}H_{28}ClN_3O_2$ (474.00): C, 70.95; H, 5.95; N, 8.87 found: C, 71.12; H, 6.07; N, 9.12.

2.1.1.10. 2-(4-(4-Chlorophenyl)piperazin-1-yl)-N-(4-(3-(4-methoxyphenyl)acryloyl)phenyl)acetamide (4j). Yellow powder (87% yield, 0.43 g), mp 158–160 °C. ^{1}H NMR (400 MHz, DMSO-d_6) δ 10.13 (s, 1H), 8.13 (d, J = 12 Hz, 2H), 7.85–7.79 (m, 5H), 7.70 (d, J = 15.5 Hz, 1H), 7.22 (d, J = 9.2 Hz, 2H), 7.02 (d, J = 12 Hz, 2H), 6.94 (d, J = 9.2 Hz, 2H), 3.82 (s, 3H), 3.34 (s, 2H), 3.20 (t, J = 5.1 Hz, 3H), 2.67 (d, J = 9.9 Hz, 1H); ^{13}C NMR (101 MHz, DMSO) δ 187.42, 168.84, 161.27, 149.79, 143.38, 143.34, 142.87, 142.80, 132.72, 130.70, 129.80, 129.67, 129.61, 128.60, 127.42, 122.29, 119.44, 118.91, 118.78, 116.84, 114.39, 62.00, 61.64, 55.37, 52.47, 47.90. Anal. calcd for $C_{28}H_{28}ClN_3O_3$ (490.00): C, 68.63; H, 5.76; N, 8.58 found: C, 68.85; H, 5.69; N, 8.77.

2.1.1.11. 2-(4-(4-Chlorophenyl)piperazin-1-yl)-N-(4-(3-(3,4,5-trimethoxyphenyl)acryloyl)phenyl)acetamide (4k). Yellow powder (77% yield, 0.42 g), mp 185–187 °C. ^{1}H NMR (400 MHz, DMSO-d_6) δ 10.16 (s, 1H), 8.18 (d, J = 8.5 Hz, 1H), 7.93–7.85 (m, 2H), 7.68 (d, J = 15.5 Hz, 1H), 7.22 (d, J = 6.7 Hz, 2H), 6.96–6.92 (m, 1H), 3.87 (s, 3H), 3.72 (s, 2H), 3.34 (s, 1H), 3.19 (d, J = 5.3 Hz, 2H), 2.67 (d, J = 5.2 Hz, 2H); ^{13}C NMR (101 MHz, DMSO) δ 187.50, 168.89, 153.12, 149.79, 143.94, 143.05, 139.67, 132.56, 130.34, 129.83, 128.61, 122.31, 121.12, 118.91, 118.78, 116.84, 106.49, 61.67, 60.14, 56.14, 52.49, 47.91. Anal. calcd for $C_{30}H_{32}ClN_3O_5$ (550.05): C, 65.51; H, 5.86; N, 7.64 found: C, 65.34; H, 5.98; N, 7.90.

2.1.1.12. N-(4-(3-(4-Bromophenyl)acryloyl)phenyl)-2-(4-(4-chlorophenyl)piperazin-1-yl)acetamide (4l). Yellow powder (81% yield, 0.44 g), mp 200–202 °C. ^{1}H NMR (400 MHz, DMSO-d_6) δ 10.18 (s, 1H), 8.16 (d, J = 8.3 Hz, 1H), 7.98 (d, J = 15.6 Hz, 1H), 7.86 (t, J = 9.1 Hz, 2H), 7.71–7.63 (m, 2H), 7.21 (d, J = 8.7 Hz, 1H), 6.93 (d, J = 8.6 Hz, 1H), 3.26 (s, 1H), 3.19 (t, J = 5.0 Hz, 2H), 2.67 (t, J = 4.8 Hz, 2H); ^{13}C NMR (101 MHz, DMSO) δ 187.42, 168.92, 149.78, 143.23, 141.99, 134.09, 132.30, 131.85, 130.72, 129.87, 128.68, 128.59, 123.82, 122.76, 122.30, 118.81, 117.40, 116.83, 61.60, 52.46, 47.91. Anal. calcd for $C_{27}H_{25}BrClN_3O_2$ (538.87): C, 60.18; H, 4.68; N, 7.80 found: C, 60.36; H, 4.90; N, 8.04.

2.1.1.13. 2-(4-(4-Chlorophenyl)piperazin-1-yl)-N-(4-(3-(2,4dichlorophenyl)acryloyl)phenyl)acetamide (4m). Yellow powder (73% yield, 0.38 g), mp 180–182 °C. ^{1}H NMR (400 MHz, DMSO-d_6) δ 10.23 (s, 1H), 8.26 (d, J = 8.6 Hz, 4H), 8.17 (dd, J = 8.7, 3.0 Hz, 7H), 8.03 (d, J = 15.6 Hz, 4H), 7.98–7.84 (m, 11H), 7.74 (d, J = 2.2 Hz, 4H), 7.55 (dd, J = 8.5, 2.1 Hz, 4H), 7.26–7.17 (m, 7H), 6.98–6.90 (m, 6H), 3.26 (s, 6H), 3.20 (t, J = 5.1 Hz, 12H), 2.67 (t, J = 5.0 Hz, 11H); ^{13}C NMR (101 MHz, DMSO) δ 187.16, 168.96, 149.79, 143.42, 136.68, 136.64, 135.49, 135.08, 132.02, 131.47, 130.15, 130.03, 129.98, 129.80, 129.48, 128.69, 128.60, 127.93, 125.28, 122.30, 118.94, 118.82, 117.41, 116.84, 61.61, 52.46, 48.02, 47.91. Anal. calcd for $C_{27}H_{24}Cl_3N_3O_2$ (528.86): C, 61.32; H, 4.57; N, 7.95 found: C, 61.45; H, 4.68; N, 8.16.

2.1.1.14. 2-(4-(4-Chlorophenyl)piperazin-1-yl)-N-(4-(3-(furan-2-yl)acryloyl)phenyl)acetamide (4n). Yellow powder (70% yield, 0.31 g), mp 207–209 °C. ^{1}H NMR (400 MHz, DMSO-d_6) δ 10.15 (s, 1H), 8.10–8.06 (m, 2H), 7.92 (d, J = 1.8 Hz, 1H), 7.85 (d, J = 8.5 Hz, 2H), 7.56 (s, 2H), 7.25–7.22 (m, 2H), 7.10 (d, J = 3.4 Hz, 1H), 6.98–6.93 (m, 2H), 6.70 (dd, J = 3.4, 1.8 Hz, 1H), 3.33–3.16 (m, 8H), 2.68 (d, J = 10.0 Hz, 5H); ^{13}C NMR (101 MHz, DMSO) δ 186.99, 168.87, 151.22, 149.80, 146.07, 143.02, 132.38, 129.97, 129.59, 129.53, 128.60, 122.30, 119.01, 118.89, 118.69, 118.65, 116.85, 116.78, 116.72, 113.09, 61.64, 52.47, 47.91. Anal. calcd

for $C_{25}H_{24}ClN_3O_3$ (449.94): C, 66.74; H, 5.38; N, 9.34 found: C, 66.53; H, 5.60; N, 9.45.

2.1.2. General method for synthesis of N-(4-(1-acetyl-5-substituted phenyl-4,5-dihydro-1H-pyrazol-3-yl)phenyl)-2-(4-(4-substituted phenyl)piperazin-1-yl)acetamide (5a–n). Compound 4a–n (1 mmol) was dissolved in acetic acid (15 mL), hydrazine hydrate (0.16 mL, 5 mmol) was added, and the solution was stirred at reflux for 3 h. The reaction mixture was poured over crushed ice (100 mL), and the precipitate was collected by vacuum filtration, washed with water, and allowed to air-dry for 24 h to yield the pure 5a–n.

2.1.2.1. N-(4-(1-Acetyl-5-phenyl-4,5-dihydro-1H-pyrazol-3-yl)phenyl)-2-(4-(4-methoxyphenyl)piperazin-1-yl)acetamide (5a). White powder (83% yield, 0.42 g), mp 135–137 °C. ^{1}H NMR (400 MHz, DMSO-d_6) δ 10.27 (s, 1H), 7.78–7.65 (m, 4H), 7.33–7.22 (m, 5H), 6.90 (d, J = 9.1 Hz, 2H), 6.83 (d, J = 9 Hz, 2H), 5.54 (dd, J = 17.9, 3.6 Hz, 1H), 3.84 (dd, J = 18.0, 11.9, 1H), 3.69 (s, 3H), 3.22 (s, 2H), 3.09 (m, 5H), 2.68 (t, J = 4.9 Hz, 4H), 2.31 (s, 3H); ^{13}C NMR (101 MHz, DMSO) δ 168.54, 167.22, 153.84, 149.80, 142.49, 140.51, 128.64, 128.60, 127.33, 127.15, 125.39, 122.28, 119.32, 119.25, 116.84, 61.59, 59.76, 55.65, 52.48, 50.20, 42.64, 22.15. Anal. calcd for $C_{30}H_{33}N_5O_3$ (511.26): C, 70.43; H, 6.50; N, 13.69 found: C, 70.29; H, 6.63; N, 13.91.

2.1.2.2. N-(4-(1-Acetyl-5-(p-tolyl)-4,5-dihydro-1H-pyrazol-3-yl)phenyl)-2-(4-(4-methoxy-phenyl)piperazin-1-yl)acetamide (5b). Yellowish white powder (75% yield, 0.39 g), mp 130–132 °C. ^{1}H NMR (400 MHz, DMSO-d_6) δ 10.04 (s, 1H), 7.79–7.62 (m, 4H), 7.12 (d, J = 7.9 Hz, 2H), 7.05 (d, J = 8.2 Hz, 2H), 6.89 (d, J = 8 Hz, 2H), 6.82 (d, J = 8 Hz, 2H), 5.52 (dd, J = 17.9, 3.6 Hz, 1H), 3.79 (dd, J = 17.9, 11.6 Hz, 1H), 3.68 (s, 3H), 3.39 (dd, J = 17.9, 3.6 Hz, 1H), 3.21 (s, 2H), 3.08 (t, J = 6.1 Hz, 4H), 2.67 (t, J = 6.1 Hz, 4H), 2.28 (s, 3H), 2.25 (s, 3H); ^{13}C NMR (101 MHz, DMSO) δ 169.07, 167.67, 154.34, 153.36, 145.84, 140.93, 140.00, 136.76, 129.59, 127.76, 125.81, 119.73, 119.24, 117.85, 114.70, 62.16, 59.55, 55.62, 53.26, 49.95, 42.57, 22.15, 21.06. Anal. calcd for $C_{31}H_{35}N_5O_3$ (525.65): C, 70.83; H, 6.71; N, 13.32 found: C, 70.98; H, 6.82; N, 13.59.

2.1.2.3. N-(4-(1-Acetyl-5-(4-methoxyphenyl)-4,5-dihydro-1H-pyrazol-3-yl)phenyl)-2-(4-(4-methoxyphenyl)piperazin-1-yl)acetamide (5c). White powder (71% yield, 0.37 g), mp 210–212 °C. ^{1}H NMR (400 MHz, DMSO-d_6) δ 10.08 (s, 1H), 7.80–7.64 (m, 4H), 7.09 (d, J = 8 Hz, 2H), 6.81–6.90 (m, 4H), 6.82 (d, J = 8 Hz, 2H), 5.51 (dd, J = 17.9, 3.6 Hz, 1H), 3.84 (dd, J = 17.9, 11.6 Hz, 1H), 3.72 (dd, J = 17.9, 3.6 Hz, 1H), 3.71 (s, 3H), 3.68 (s, 3H), 3.22 (s, 2H), 3.08 (t, J = 4.9 Hz, 4H), 2.67 (t, J = 4.9 Hz, 4H), 2.27 (s, 3H); ^{13}C NMR (101 MHz, DMSO) δ 168.53, 167.66, 162.82, 158.84, 154.34, 153.36, 145.85, 134.98, 127.76, 127.19, 126.50, 119.73, 119.25, 117.85, 114.71, 114.42, 62.15, 59.26, 55.63, 55.53, 53.26, 49.95, 42.54, 20.89. Anal. calcd for $C_{31}H_{35}N_5O_4$ (541.65): C, 68.74; H, 6.51; N, 12.93 found: C, 69.01; H, 6.67; N, 13.15.

2.1.2.4. N-(4-(1-Acetyl-5-(3,4,5-trimethoxyphenyl)-4,5-dihydro-1H-pyrazol-3-yl)phenyl)-2-(4-(4-methoxyphenyl)piperazin-1-yl)acetamide (5d). Whitish brown powder (80% yield, 0.48 g), mp 117–119 °C. ^{1}H NMR (400 MHz, DMSO-d_6) δ 10.08 (s, 1H), 7.79–7.65 (m, 4H), 6.90 (d, J = 9.1 Hz, 2H), 6.82 (d, J = 9.1 Hz, 2H), 6.45 (s, 2H), 5.45 (dd, J = 17.9, 3.6 Hz, 1H), 3.78 (dd, J = 17.9,

11.6 Hz, 1H), 3.72 (dd, J = 17.9, 3.6 Hz, 1H), 3.72 (s, 6H), 3.68 (s, 3H), 3.62 (s, 3H), 3.22 (s, 2H), 3.07 (t, J = 4.9 Hz, 4H), 2.66 (t, J = 4.9 Hz, 4H), 2.32 (s, 3H); ^{13}C NMR (101 MHz, DMSO) δ 168.48, 167.97, 153.51, 153.36, 145.85, 138.73, 136.98, 127.82, 119.74, 119.25, 117.85, 114.71, 102.94, 60.37, 59.99, 56.31, 55.63, 53.25, 49.95, 42.67, 20.90. Anal. calcd for $C_{33}H_{39}N_5O_6$ (601.70): C, 65.87; H, 6.53; N, 11.64 found: C, 66.09; H, 6.62; N, 11.91.

2.1.2.5. N-(4-(1-Acetyl-5-(4-bromophenyl)-4,5-dihydro-1H-pyrazol-3-yl)phenyl)-2-(4-(4-methoxyphenyl)piperazin-1-yl)acetamide (5e). White powder (72% yield, 0.42 g), mp 118–120 °C. ^{1}H NMR (400 MHz, DMSO-d_6) δ 9.98 (s, 1H), 7.80–7.68 (m, 4H), 7.51 (d, J = 8.4 Hz, 2H), 7.15 (d, J = 8.4 Hz, 2H), 6.89 (d, J = 9.1 Hz, 2H), 6.81 (d, J = 9.1 Hz, 2H), 5.51 (dd, J = 11.8, 4.6 Hz, 1H), 3.86 (dd, J = 18.0, 11.8 Hz, 1H), 3.82 (dd, J = 18.0, 4.6 Hz, 1H), 3.68 (s, 3H), 3.21 (s, 2H), 3.04 (t, J = 4.9 Hz, 4H), 2.67 (t, J = 4.9 Hz, 4H), 2.29 (s, 3H); ^{13}C NMR (101 MHz, DMSO) δ 169.42, 167.91, 153.37, 145.83, 142.25, 140.92, 131.98, 128.29, 127.85, 125.41, 120.76, 119.75, 117.88, 114.72, 62.16, 55.64, 53.25, 49.94, 43.98, 22.11. Anal. calcd for $C_{30}H_{32}BrN_5O_3$ (590.52): C, 61.02; H, 5.46; N, 11.86 found: C, 60.97; H, 5.65; N, 12.04.

2.1.2.6. N-(4-(1-Acetyl-5-(2,4-dichlorophenyl)-4,5-dihydro-1H-pyrazol-3-yl)phenyl)-2-(4-(4-methoxyphenyl)piperazin-1-yl)acetamide (5f). Yellow powder (73% yield, 0.41 g), mp 160–162 °C. ^{1}H NMR (400 MHz, DMSO-d_6) δ 10.00 (s, 1H), 7.77–7.63 (m, 3H), 7.37 (d, J = 8.3, Hz, 2H), 7.08 (d, J = 8.4 Hz, 2H), 6.89 (d, J = 9.1 Hz, 2H), 6.81 (d, J = 9.0 Hz, 2H), 5.70 (dd, J = 12.1, 5.1 Hz, 1H), 3.91 (dd, J = 17.9, 12.0 Hz, 1H), 3.87 (dd, J = 12.1, 5.1 Hz, 1H), 3.68 (s, 3H), 3.21 (s, 2H), 3.08 (t, J = 3.3 Hz, 4H), 2.64 (t, J = 3.3 Hz, 4H), 2.34 (s, 3H); ^{13}C NMR (101 MHz, DMSO) δ 169.58, 167.95, 154.70, 150.25, 144.14, 138.64, 132.96, 132.24, 129.57, 129.06, 128.23, 127.86, 122.76, 119.71, 119.18, 117.31, 62.06, 58.53, 52.94, 48.37, 41.24, 22.05. Anal. calcd for $C_{30}H_{31}Cl_2N_5O_3$ (580.51): C, 62.07; H, 5.38; N, 12.06 found: C, 62.32; H, 5.49; N, 12.32.

2.1.2.7. N-(4-(1-Acetyl-5-(furan-2-yl)-4,5-dihydro-1H-pyrazol-3-yl)phenyl)-2-(4-(4-methoxy-phenyl)piperazin-1-yl)acetamide (5g). Whitish gray powder (79% yield, 0.39 g), mp 130–132 °C. ^{1}H NMR (400 MHz, DMSO-d_6) δ 10.08 (s, 1H), 7.79–7.70 (m, 4H), 7.57–7.52 (m, 1H), 6.89 (d, J = 9.1 Hz, 2H), 6.81 (d, J = 9.1 Hz, 2H), 6.37–6.35 (m, 1H), 6.30–6.29 (m, 1H), 5.61 (dd, J = 11.9, 4.5 Hz, 1H), 3.91 (dd, J = 17.9, 12.0 Hz, 1H), 3.87 (dd, J = 11.9, 4.5 Hz, 1H), 3.68 (s, 3H), 3.22 (s, 2H), 3.08 (t, J = 4.9 Hz, 4H), 2.67 (t, J = 4.9 Hz, 4H), 2.25 (s, 3H); ^{13}C NMR (101 MHz, DMSO) δ 169.12, 167.82, 154.47, 153.36, 153.30, 145.85, 142.70, 141.01, 127.76, 126.30, 119.75, 117.86, 114.71, 110.91, 107.34, 62.15, 55.64, 53.38, 53.26, 49.95, 38.87, 22.15. Anal. calcd for $C_{30}H_{31}Cl_2N_5O_3$ (580.51): C, 67.07; H, 5.38; N, 13.06 found: C, 62.29; H, 5.92; N, 13.48.

2.1.2.8. N-(4-(1-Acetyl-5-phenyl-4,5-dihydro-1H-pyrazol-3-yl)phenyl)-2-(4-(4-chloro-phenyl)piperazin-1-yl)acetamide (5h). White powder (83% yield, 0.43 g), mp 186–188 °C. ^{1}H NMR (400 MHz, DMSO-d_6) δ 10.07 (s, 1H), 7.80–7.69 (m, 4H), 7.36–7.23 (m, 5H), 7.27–7.17 (d, J = 8 Hz, 2H), 6.95 (d, J = 9.1 Hz, 2H), 5.52 (dd, J = 11.8, 4.5 Hz, 1H), 3.86 (dd, J = 17.9, 11.6 Hz, 1H), 3.23–3.16 (m, 6H), 3.10 (dd, J = 18.0, 4.6 Hz, 1H), 2.66 (t, J = 5.0 Hz, 4H), 2.30 (s, 3H); ^{13}C NMR (101 MHz, DMSO) δ 169.02, 167.74, 154.31, 150.25, 142.94, 140.97, 129.10, 129.06, 127.78, 127.61, 126.44,

125.85, 122.77, 119.74, 117.30, 62.04, 59.79, 52.94, 48.38, 42.63, 22.16. Anal. calcd for $C_{29}H_{30}ClN_5O_2$ (516.04): C, 67.50; H, 5.86; N, 13.57 found: C, 67.73; H, 5.92; N, 13.70.

2.1.2.9. N-(4-(1-Acetyl-5-(p-tolyl)-4,5-dihydro-1H-pyrazol-3-yl)phenyl)-2-(4-(4-chloro-phenyl)piperazin-1-yl)acetamide (5i). White powder (66% yield, 0.35 g), mp 150–152 °C. ^{1}H NMR (400 MHz, DMSO-d_6) δ 9.76 (s, 5H), 7.79–7.64 (m, 4H) 7.23 (d, J = 8 Hz, 2H), 7.12 (d, J = 7.9 Hz, 2H), 7.05 (d, J = 7.8 Hz, 2H), 6.95 (d, J = 8 Hz, 2H), 5.47 (dd, J = 11.6, 3.9 Hz, 1H), 3.79 (dd, J = 17.9, 11.7 Hz, 1H), 3.20–3.18 (m, 6H), 3.06 (dd, J = 17.9, 4.8 Hz, 1H), 2.66 (t, J = 6.1 Hz, 4H), 2.28 (s, 3H), 2.25 (s, 3H); ^{13}C NMR (101 MHz, DMSO) δ 169.02, 167.70, 154.35, 150.24, 141.57, 140.86, 139.98, 136.78, 129.60, 129.06, 127.80, 127.76, 126.53, 125.80, 122.78, 119.76, 119.24, 117.31, 62.06, 59.54, 52.94, 48.37, 42.57, 22.15, 21.06. Anal. calcd for $C_{30}H_{32}ClN_5O_2$ (530.07): C, 67.98; H, 6.09; N, 13.21 found: C, 68.15; H, 6.21; N, 13.48.

2.1.2.10. N-(4-(1-Acetyl-5-(4-methoxyphenyl)-4,5-dihydro-1H-pyrazol-3-yl)phenyl)-2-(4-(4-chlorophenyl)piperazin-1-yl)acetamide (5j). Yellow powder (67% yield, 0.36 g), mp 220–222 °C. ^{1}H NMR (400 MHz, DMSO-d_6) δ 10.01 (s, 1H), 7.76–7.66 (m, 4H), 7.22 (d, J = 9.0 Hz, 2H), 7.09 (d, J = 8.5 Hz, 2H), 6.95 (d, J = 9.0 Hz, 2H), 6.87 (d, J = 8.7 Hz, 2H), 5.52 (dd, J = 18.0, 4.9 Hz, 1H), 3.78 (dd, J = 18.0, 11.4 Hz, 1H), 3.71 (s, 3H), 3.24–3.16 (m, 6H), 3.08 (dd, J = 17.9, 4.9 Hz, 1H), 2.66 (t, J = 5.0 Hz, 4H), 2.27 (s, 3H); ^{13}C NMR (101 MHz, DMSO) δ 169.04, 167.74, 158.83, 154.35, 150.23, 140.85, 134.95, 129.06, 127.79, 127.76, 127.18, 126.55, 122.79, 119.77, 119.26, 117.30, 114.41, 62.04, 59.27, 55.52, 52.93, 48.37, 42.53, 22.16. Anal. calcd for $C_{30}H_{32}ClN_5O_2$ (530.07): C, 67.98; H, 6.09; N, 13.21 found: C, 68.16; H, 6.07; N, 12.95.

2.1.2.11. N-(4-(1-Acetyl-5-(3,4,5-trimethoxyphenyl)-4,5-dihydro-1H-pyrazol-3-yl)phenyl)-2-(4-(4-chlorophenyl)piperazin-1-yl)acetamide (5k). White powder (63% yield, 0.34 g), mp 162–164 °C. ^{1}H NMR (400 MHz, DMSO-d_6) δ 10.00 (s, 1H), 7.79–7.62 (m, 4H), 7.22 (d, J = 9.0 Hz, 2H), 6.95 (d, J = 9.0 Hz, 2H), 6.45 (s, 2H), 5.52 (dd, J = 18.0, 5.3 Hz, 1H), 3.86 (dd, J = 17.9, 11.6 Hz, 1H), 3.72 (s, 6H), 3.62 (s, 3H), 3.22–3.19 (m, 6H), 3.12 (dd, J = 18.0, 5.3 Hz, 1H), 2.66 (t, J = 4.9 Hz, 4H), 2.32 (s, 3H); ^{13}C NMR (101 MHz, DMSO) δ 169.04, 168.05, 154.45, 153.51, 150.23, 140.85, 138.70, 136.98, 129.05, 127.81, 126.51, 122.79, 119.77, 117.30, 102.92, 62.04, 60.37, 60.00, 56.29, 52.93, 48.36, 42.67, 22.16. Anal. calcd for $C_{32}H_{36}ClN_5O_5$ (606.12): C, 63.41; H, 5.99; N, 11.55 found: C, 63.59; H, 6.14; N, 11.79.

2.1.2.12. N-(4-(1-Acetyl-5-(4-bromophenyl)-4,5-dihydro-1H-pyrazol-3-yl)phenyl)-2-(4-(4-chlorophenyl)piperazin-1-yl)acetamide (5l). White powder (83% yield, 0.42 g), mp 110–112 °C. ^{1}H NMR (400 MHz, DMSO-d_6) δ 10.02 (s, 1H), 7.79–7.64 (m, 4H), 7.51 (d, J = 8.0 Hz, 2H), 7.22 (d, J = 8.5 Hz, 2H), 7.15 (d, J = 8.1 Hz, 2H), 6.95 (d, J = 8.5 Hz, 2H), 5.51 (dd, J = 11.9, 4.5 Hz, 1H), 3.83 (dd, J = 18.1, 11.5 Hz, 1H), 3.21 (m, 6H), 3.11 (dd, J = 18.1, 4.9 Hz, 1H), 2.66 (t, J = 5.0 Hz, 4H), 2.29 (s, 3H); ^{13}C NMR (101 MHz, DMSO) δ 169.13, 169.01, 167.83, 154.31, 150.24, 142.26, 140.97, 131.97, 129.06, 128.29, 127.82, 126.35, 122.79, 120.63, 119.74, 119.21, 117.30, 62.07, 59.29, 52.95, 48.38, 42.35, 22.13. Anal. calcd for $C_{29}H_{29}BrClN_5O_2$ (594.94): C, 58.55; H, 4.91; N, 11.77 found: C, 58.34; H, 5.12; N, 11.95.

2.1.2.13. N-(4-(1-Acetyl-5-(2,4-dichlorophenyl)-4,5-dihydro-1H-pyrazol-3-yl)phenyl)-2-(4-(4-chlorophenyl)piperazin-1-yl)acetamide (5m). Yellowish white powder (73% yield, 0.38 g), mp 155–157 °C. ^{1}H NMR (400 MHz, DMSO-d_6) δ 10.00 (s, 1H), 7.79–7.63 (m, 3H), 7.37 (dd, J = 8.4, 2.2 Hz, 2H), 7.22 (d, J = 9.0 Hz, 2H), 7.08 (d, J = 8.4 Hz, 2H), 6.94 (d, J = 9.0 Hz, 2H), 5.70 (dd, J = 12.1, 5.1 Hz, 1H), 3.90 (dd, J = 18.0, 12.0 Hz, 1H), 3.21–3.18 (m, 6H), 3.05 (dd, J = 17.9, 5.3 Hz, 1H), 2.66 (t, J = 5.0 Hz, 3H), 2.34 (s, 3H); ^{13}C NMR (101 MHz, DMSO) δ 169.05, 167.94, 154.52, 154.49, 153.37, 145.84, 141.74, 141.03, 138.63, 132.97, 132.24, 129.56, 128.21, 127.85, 126.18, 119.68, 119.17, 117.84, 114.70, 62.19, 57.29, 55.62, 53.28, 49.95, 41.23, 22.04. Anal. calcd for $C_{29}H_{28}Cl_3N_5O_2$ (584.93): C, 59.55; H, 4.83; N, 11.97 found: C, 59.76; H, 4.97; N, 12.86.

2.1.2.14. N-(4-(1-Acetyl-5-(furan-2-yl)-4,5-dihydro-1H-pyrazol-3-yl)phenyl)-2-(4-(4-chlorophenyl)piperazin-1-yl)acetamide (5n). Whitish gray powder (79% yield, 0.39 g), mp 124–126 °C. ^{1}H NMR (400 MHz, DMSO-d_6) δ 10.00 (s, 1H), 7.80–7.65 (m, 4H), 7.54 (d, J = 3.3 Hz, 1H), 7.23 (d, J = 8.6 Hz, 2H), 6.95 (d, J = 8.8 Hz, 2H), 6.38 (t, J = 2.5 Hz, 1H), 6.30 (d, J = 3.3 Hz, 1H), 5.61 (dd, J = 11.8, 4.4 Hz, 1H), 3.69 (dd, J = 15.3, 11.8 Hz, 1H), 3.22–3.19 (m, 7H), 2.67 (t, J = 5.0 Hz, 4H), 2.25 (s, 3H); ^{13}C NMR (101 MHz, DMSO) δ 169.01, 167.79, 154.42, 153.31, 150.25, 142.69, 140.94, 129.06, 127.81, 127.77, 126.36, 122.78, 119.76, 117.31, 110.91, 107.33, 62.08, 53.39, 52.96, 48.38, 38.87, 22.16. Anal. calcd for $C_{27}H_{28}ClN_5O_3$ (506.00): C, 64.09; H, 5.58; N, 13.84 found: C, 63.87; H, 5.74; N, 14.09.

2.2. Biological evaluation

2.2.1. Antiproliferative assay. The antiproliferative activity of compounds **4a–n** and **5a–n** against four human cancer cell lines (colon – HCT-116, prostatic – PC-3, breast – MCF-7, and pancreatic – MDAMB-231, the cell line was obtained from ATCC *via* Holding company for biological products and vaccines (VACSERA), Cairo, Egypt) was investigated using the MTT assay.[20,29] Doxorubicin and sorafenib was utilized as controls in this study. See ESI Appendix A† for more details.

2.2.2. EGFR inhibitory assay. Compounds **4n**, **5d**, and **5g** were further tested for their ability to target the EGFR-TK, which is a probable target for their effective antiproliferative activity. The IC_{50} value for each compound was calculated and compared to erlotinib, which served as a ref. 27. See ESI Appendix A† for more details.

2.2.3. HER2 inhibitory assay. Compounds **4n**, **5d**, and **5g** were further tested for their inhibitory action against HER2-TK using lapatinib as a reference drug.[30] Refer to ESI Appendix A† for more details.

2.2.4. Cell cycle analysis and apoptosis. Compound **5d** (after 24 hours of treatment at 25 μM) was evaluated for its impact on the cell cycle of MDA-MB 231 cancer cells.[31] See ESI Appendix A† for more details.

2.3. Molecular docking study and molecular dynamics simulation

All experimental methods, data, and tools for molecular docking and MD simulation were submitted in ESI Appendix A.†

3. Results and discussion

3.1. Chemistry

Scheme 1 details the synthesis of the target compounds **4a–n** and **5a–n**. Chalcones **1a–g** and their chloroacetamide derivatives **2a–g** were synthesized using the typical base-catalyzed Claisen–Schmidt condensation of various aromatic aldehydes with 4-aminoacetophenone,[32] then acetylated the free amino group using chloroacetyl chloride.[33] Acetylation was an effective approach for incorporating a spacer group into the chalcone molecule. Compounds **4a–n** were prepared by alkylating substituted *N*-phenylpiperazines **3a–b** with compounds **2a–g** in DMF, which contains K_2CO_3 as a base,[34] Scheme 1.
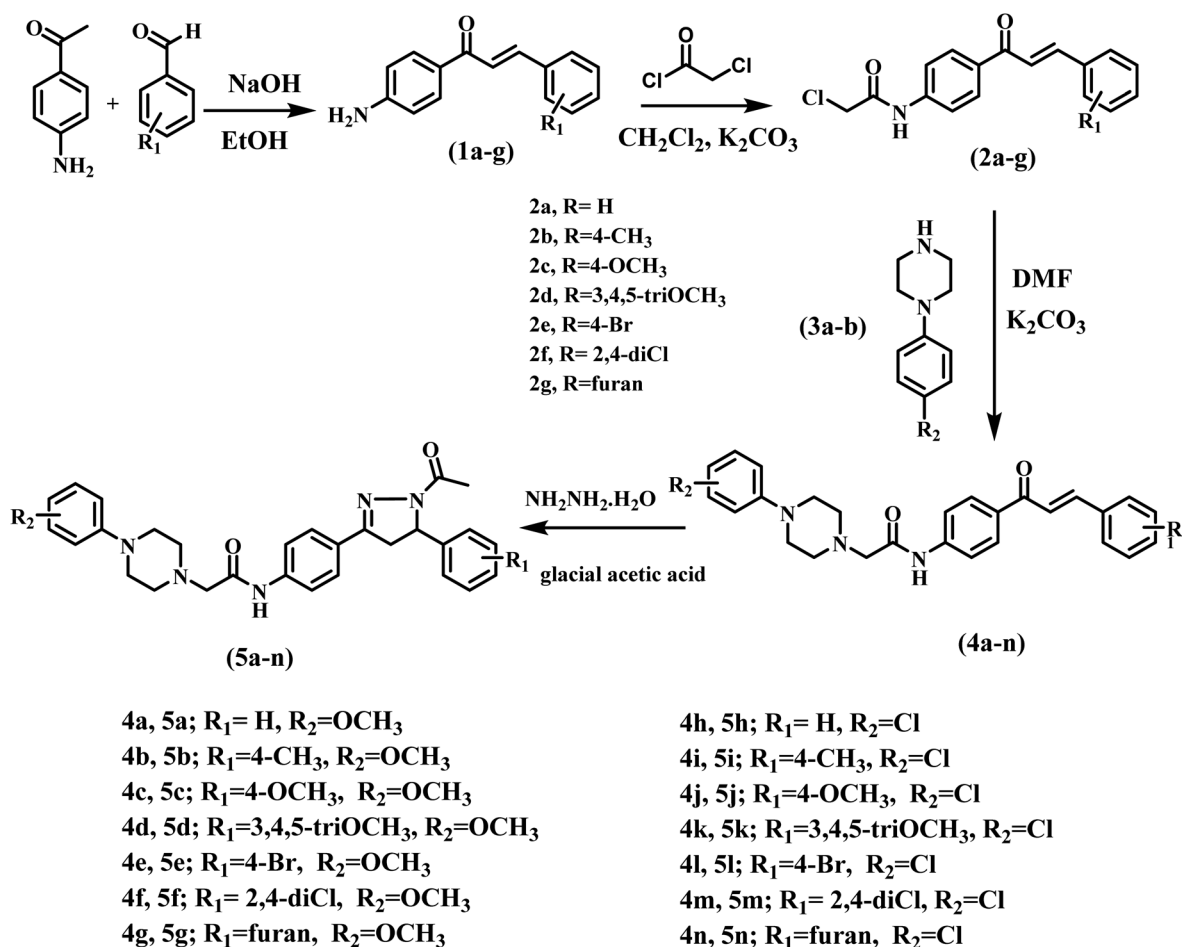
Compounds **4a–n** were validated using ^1H NMR, ^{13}C NMR, and elemental analysis. Compounds **4a–n** exhibited distinct and significant signals at various chemical shifts in their ^1H NMR spectra. We observe the NH-group at approximately δ 9.50–10.60 ppm. Also, the CH=CH bond, which is known to be an important part of chalcones, showed clear doublet peaks in the chemical shift range of δ 6.8–6.9 ppm, along with a coupling constant of 15.6–16 Hz, which shows that the chalcone double bond is in a trans configuration. Two protons corresponding to the CH_2 group of the acetamide spacer were identified through a singlet signal at δ 3.25–3.36 ppm.

Additionally, piperazine protons exhibited two prominent triplet peaks at δ 2.60–2.67 and δ 3.18–3.21 ppm. The ^{13}C NMR of **4a–n** showed two prominent signals at δ 167 and 187 ppm, corresponding to the amidic carbonyl and ketonic carbonyl of the chalcone moiety, respectively.

Scheme 1 illustrates the reaction of compound **4a–n** with hydrazine hydrate to synthesize compounds **5a–n**.[35] The ^1H NMR spectra of *N*-acetyl pyrazolines **5a–n** showed different peaks that were the protons of the cyclized forms CH and CH_2. These peaks showed up as doublets of doublets in three different areas at δ 3.08–3.10, 3.84–3.90, and 5.52–5.55 ppm. The ^{13}C NMR spectrum of **5a–n** showed the absence of chalcone's ketonic carbonyl and the presence of amidic carbonyl at δ 168 ppm.

3.2. Biological evaluation

3.2.1. Cell viability assay.
The cell viability effect of compounds **4a–n** and **5a–n** was assessed utilizing the MCF-10A normal human mammary gland epithelial cell line. We assessed the cell viability of compounds **4a–n** and **5a–n** using the MTT test after four days of treatment with MCF-10A cells.[36] Tables 1 and 2 demonstrate that none of the investigated compounds displayed cytotoxicity, with all hybrids sustaining over 82% cell viability at a concentration of 50 μM.

2a, R= H
2b, R=4-CH₃
2c, R=4-OCH₃
2d, R=3,4,5-triOCH₃
2e, R=4-Br
2f, R= 2,4-diCl
2g, R=furan

4a, 5a; R₁= H, R₂=OCH₃
4b, 5b; R₁=4-CH₃, R₂=OCH₃
4c, 5c; R₁=4-OCH₃, R₂=OCH₃
4d, 5d; R₁=3,4,5-triOCH₃, R₂=OCH₃
4e, 5e; R₁=4-Br, R₂=OCH₃
4f, 5f; R₁= 2,4-diCl, R₂=OCH₃
4g, 5g; R₁=furan, R₂=OCH₃

4h, 5h; R₁= H, R₂=Cl
4i, 5i; R₁=4-CH₃, R₂=Cl
4j, 5j; R₁=4-OCH₃, R₂=Cl
4k, 5k; R₁=3,4,5-triOCH₃, R₂=Cl
4l, 5l; R₁=4-Br, R₂=Cl
4m, 5m; R₁= 2,4-diCl, R₂=Cl
4n, 5n; R₁=furan, R₂=Cl

Scheme 1 Synthesis of targeted compounds **4a–n** and **5a–n**.

Table 1 IC$_{50}$s of compounds **4a–n**, doxorubicin, and sorafenib against four cancer cell lines[a]

Scaffold A compounds (4a-n)

| Compd | Cell viability% | Antiproliferative activity IC$_{50}$ ± SEM (nM) | | | | GI$_{50}$ (average IC$_{50}$) |
		HCT-116	MCF-7	MDAMB-231	PC-3	
4a	89	68.64 ± 3.7	72.43 ± 3.7	58.74 ± 3.1	78.23 ± 4.0	70
4b	90	79.64 ± 3.8	65.48 ± 3.5	77.25 ± 3.9	31.98 ± 2.1	64
4c	92	18.09 ± 1.4	28.32 ± 1.8	23.12 ± 1.7	34.51 ± 2.1	26
4d	87	29.11 ± 1.9	24.23 ± 1.7	15.46 ± 1.3	61.42 ± 3.5	32
4e	90	64.81 ± 3.5	52.45 ± 2.9	43.63 ± 2.5	73.93 ± 3.8	59
4f	86	>100	>100	88.64 ± 4.4	>100	100
4g	82	17.31 ± 1.4	9.37 ± 0.7	8.51 ± 0.7	14.15 ± 1.2	12
4h	85	49.56 ± 2.8	41.34 ± 2.4	32.83 ± 2.3	20.37 ± 1.5	36
4i	89	86.09 ± 4.3	91.60 ± 4.6	81.58 ± 4.1	>100	90
4j	91	27.44 ± 1.9	42.93 ± 2.5	38.72 ± 2.3	66.85 ± 3.5	44
4k	89	34.76 ± 2.2	17.86 ± 1.4	19.95 ± 1.6	42.92 ± 2.5	29
4l	87	75.35 ± 4.1	80.78 ± 3.9	63.41 ± 3.4	86.36 ± 4.3	76
4m	86	44.79 ± 2.6	35.81 ± 2.2	26.36 ± 1.8	55.24 ± 3.2	41
4n	90	8.67 ± 0.9	6.94 ± 0.4	4.80 ± 0.3	9.08 ± 0.8	7
Doxorubicin	—	5.23 ± 0.3	4.17 ± 0.2	3.18 ± 0.1	8.87 ± 0.6	5
Sorafenib	—	5.47 ± 0.3	7.26 ± 0.3	7.64 ± 0.4	11.53 ± 0.9	8

[a] —: Not determined.

3.2.2. Antiproliferative assay. The antiproliferative activity of new compounds **4a–n** (scaffold A compounds) and **5a–n** (scaffold B compounds) against four human cancer cell lines (colon – HCT-116, prostatic – PC-3, breast – MCF-7, and pancreatic – MDAMB-231) was investigated using the MTT assay.[20,29] Doxorubicin and sorafenib was utilized as controls in this study. Tables 1 and 2 present the median inhibitory concentration (IC$_{50}$) and GI$_{50}$ (average IC$_{50}$) values for the four cancer cell lines.
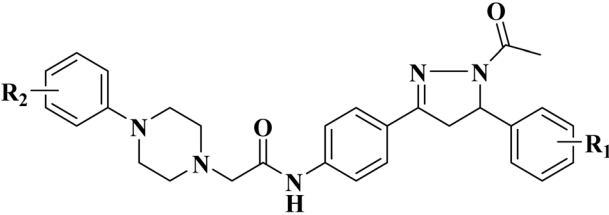
The antiproliferative activity of scaffold A (chalcone-based) compounds **4a–n** was generally weak to moderate, with GI$_{50}$ values ranging from 7 to 100 μM against the four examined cancer cell lines. In comparison, the standard doxorubicin had a GI$_{50}$ value of 5 μM, while sorafenib had a GI50 value of 8 μM. Compounds **4c**, **4d**, **4g** and **4n** exhibited the highest potency among the derivatives, with GI$_{50}$ values ranging from 7 to 32 μM. Compounds **4g** and **4n** (GI$_{50}$ = 12 and 7 μM, respectively) demonstrated equivalent potency to the reference drugs doxorubicin and sorafenib. Among the newly synthesized derivatives **4a–n**, compound **4n** (R$_1$ = furan-2-yl, R$_2$ = Cl, scaffold A) had the highest potency with a GI$_{50}$ value of 7 μM. It showed similar potency to doxorubicin (GI$_{50}$ = 5 μM) and sorafenib (GI$_{50}$ = 8 μM). Compound **4n** outperformed the reference drug sorafenib against the two types of breast cancer cells, MCF-7 and MDAMB-231, with IC$_{50}$ values of 6.94 and 4.80 μM, respectively.

Sorafenib had IC$_{50}$ values of 7.26 and 7.64 μM for the same cell lines. These results showed that compound **4n** was 1.6 times more potent than sorafenib against the breast cancer MDAMB-231 cell line, nevertheless, compound **4n** exhibits lower potency than doxorubicin against all cancer cell types.

Compound **4g** (R$_1$ = furan-2-yl, R$_2$ = OMe, scaffold A), which shares the same structure as compound **4n** but with a methoxy group at the *para* position of *N*-phenyl piperazine moiety, exhibited a GI$_{50}$ of 12 μM (1.7-fold less potent than compound **4n**). This indicates that a chlorine atom at the *para* position of *N*-phenyl piperazine moiety is more tolerated for the antiproliferative activity than a methoxy group. Compound **4g** was 2-fold less potent than **4n** against the two breast cancer cell lines MCF-7 and MDAMB-231.

Moreover, substituting the *para*-position of the phenyl group of the chalcone moiety (R$_1$) is crucial for the antiproliferative action of compounds **4a–n**. Compounds **4h–m** share the same structure as compound **4n** but with different substituents at the *para*-position of the phenyl group of the chalcone moiety. The GI$_{50}$ values of **4h–m** ranged from 29 to 90 μM, making them at least four times less potent than compound **4n** (GI$_{50}$ = 7 μM). The data suggest that the furan group at the *para*-position of the phenyl group of the chalcone moiety is crucial for activity. Still, other substituents such as H atom, methyl group, methoxy group, and halogen atoms are less well-tolerated.

Table 2 IC_{50}s of compounds **5a–n**, doxorubicin, and sorafenib against four cancer cell lines[a]

Scaffold B compounds (5a-n)

Comp.	Cell viability%	Antiproliferative activity $IC_{50} \pm$ SEM (nM)				GI_{50} (average IC_{50})
		HCT-116	MCF-7	MDAMB-231	PC-3	
5a	87	32.08 ± 2.1	19.56 ± 1.4	25.70 ± 1.7	46.29 ± 2.5	31
5b	89	24.93 ± 1.8	13.76 ± 1.1	10.36 ± 0.9	21.92 ± 1.6	18
5c	92	18.63 ± 1.5	9.68 ± 0.8	8.21 ± 0.7	16.22 ± 1.3	13
5d	91	6.47 ± 0.4	5.05 ± 0.4	2.89 ± 0.1	12.95 ± 1.0	7
5e	86	26.75 ± 2.0	15.19 ± 1.3	19.33 ± 1.5	29.57 ± 1.9	23
5f	89	53.98 ± 3.2	47.52 ± 2.6	51.56 ± 2.8	57.80 ± 3.3	53
5g	85	8.06 ± 0.7	3.78 ± 0.2	5.97 ± 0.3	7.48 ± 0.6	6
5h	90	74.94 ± 4.1	85.42 ± 4.6	68.27 ± 3.7	87.61 ± 4.3	79
5i	89	62.51 ± 3.4	54.68 ± 3.1	56.13 ± 3.2	67.76 ± 3.6	60
5j	86	>100	94.05 ± 4.9	89.44 ± 4.3	>100	100
5k	90	52.83 ± 3.0	40.76 ± 2.4	33.82 ± 2.1	45.69 ± 2.6	43
5l	93	62.51 ± 3.4	54.68 ± 3.1	56.13 ± 3.2	67.76 ± 3.6	60
5m	91	69.88 ± 3.7	71.26 ± 3.6	64.66 ± 3.5	76.68 ± 3.9	70
5n	84	39.62 ± 2.3	23.89 ± 1.7	27.75 ± 1.8	36.82 ± 2.2	32
Doxorubicin	—	5.23 ± 0.3	4.17 ± 0.2	3.18 ± 0.1	8.87 ± 0.6	5
Sorafenib	—	5.47 ± 0.3	7.26 ± 0.3	7.64 ± 0.4	11.53 ± 0.9	7

[a] —: Not determined.

Compounds **4i** (R_1 = Me, R_2 = Cl, scaffold A) and **4l** (R_1 = Br, R_2 = Cl, scaffold A) had the highest GI_{50} values, indicating the lowest potency of the compounds **4h–m**. Their GI_{50} values were 90 and 76 μM, 13 and 11 times less potent than compound **4n** (R_1 = furan-2-yl, R_2 = Cl, scaffold A). This indicates that a methyl group and a bromine atom (R_1) are the least tolerated for antiproliferative activity.

The antiproliferative activity of scaffold B compounds, **5a–n**, was moderate to high compared to the open-ring counterparts, **4a–n** (scaffold A compounds). The compounds **5a–n** had improved GI_{50} values ranging from 6 to 79 μM, except for **5j**, which had a GI_{50} value of 100 μM (the least potent one). Compounds **5b**, **5c**, **5d**, and **5g** were found to be the most efficient derivatives with GI_{50} values of 18, 13, 7, and 6 μM, respectively, making compounds **5d** and **5g** equipotent to the references doxorubicin and sorafenib (GI_{50} values 5 and 7 μM, respectively). Compound **5d** (R_1 = 3,4,5-tri-OMe, R_2 = OMe, and scaffold B) had the highest potency among the derivatives tested against the MDAMB-231 breast cancer cell line, with an IC_{50} value of 2.89 ± 0.1 μM. It was more potent than both doxorubicin and sorafenib. Compound **5d** exhibited 2.7 times greater potency than sorafenib against the MDAMB-231 breast cancer cell line, as seen in Table 2. Compound **5g** (R_1 = furan-2-yl, R_2 = OMe, and scaffold B) demonstrated the highest efficiency

against the MCF-7 breast cancer cell line. Its IC_{50} value was measured at 3.78 ± 0.2 μM, which is lower than the IC_{50} values of doxorubicin (4.17 ± 0.2 μM) and sorafenib (7.26 ± 0.3 μM). This indicates that compound **5g** is more potent than doxorubicin and sorafenib against the MCF-7 breast cancer cell line. These *in vitro* assays suggest that compounds **5d**, **5g**, and **4n** can be anti-breast cancer agents. However, further structural modifications are necessary to enhance their potency.

Compounds **5b** (R_1 = CH₃, R_2 = OMe, and scaffold B) and **5c** (R_1 = OMe, R_2 = OMe, and scaffold B) demonstrated GI_{50} values of 18 and 13 μM, respectively being 2-folds less potent than compound **5d** and **5g**, these data indicate that the presence of furan moiety or tri-methoxy group at the *para*-position of the phenyl group of the chalcone moiety is essential for activity. Replacement of these groups (furan or tri-methoxy group) with other substituents like methyl or methoxy group resulted in a marketed decrease in the antiproliferative activity.

3.2.3. EGFR inhibitory assay. The compounds **4n**, **5d**, and **5g**, which showed the highest efficacy in reducing cell growth, were further tested for their ability to target the EGFR-TK, which is a probable target for their effective antiproliferative activity. The IC_{50} value for each compound was calculated and compared to erlotinib, which served as a ref. 27. Table 3 lists these IC_{50} values.

Table 3 IC$_{50}$ values of **4n**, **5d**, **5g**, and erlotinib against EGFR and HER2-TKs

Comp.	EGFR IC$_{50}$ ± SEM (μM)	HER2 IC$_{50}$ ± SEM (μM mL^{-1})
4n	0.799 ± 0.026	0.227 ± 0.007
5d	0.126 ± 0.004	0.061 ± 0.002
5g	1.192 ± 0.039	0.771 ± 0.025
Erlotinib	0.076 ± 0.002	—
Lapatinib	—	0.026 ± 0.001

The results of this *in vitro* assay test are consistent with the results of the antiproliferative assay. Compound **5d** (R$_1$ = 3,4,5-tri-OMe, R$_2$ = OMe, scaffold B), the most effective antiproliferative agent, was also the most effective EGFR inhibitor with an IC$_{50}$ value of 0.126 ± 0.004 μM. It was equally potent as the reference erlotinib (IC$_{50}$ value = 0.076 ± 0.002 μM). Compounds **4n** and **5g** had promising EGFR inhibitory effects, with IC$_{50}$ values of 0.799 and 1.192 μM, respectively. This means they were at least 10 times less effective as EGFR inhibitors than erlotinib. The data indicate that compound **5d** is an efficacious antiproliferative agent that may function as an EGFR inhibitor.

3.2.4. HER2 inhibitory activity. Compounds **4n**, **5d**, and **5g** were further tested for their inhibitory action against HER2-TK using lapatinib as a reference drug.[30] Results are cited in Table 3. Once again, compound **5d** was the most potent HER2 inhibitor with an IC$_{50}$ value of 0.061 ± 0.002 μM, in comparison to the reference apatinib, which had an IC$_{50}$ value of 0.026 ±

Table 4 Cell cycle analysis of MDA-MB 231 cancer cells after treatment with compound **5d** for 24 h

DNA content				
Code	% G0–G1	% S	% G2/M	Comment
5d	78.53	18.11	3.36	Cell cycle arrest @ G1
Control	64.15	24.38	11.47	—

Table 5 Apoptosis induction analysis of MDA-MB cancer cells after treatment with compound **5d** for 24 h

	Apoptosis			
Code	Total	Early	Late	Necrosis
5d	29.59	17.13	8.89	3.57
Control	2.21	0.34	0.15	1.72

0.001 μM. These *in vitro* assay data revealed that compound **5d** was an efficient antiproliferative agent that may be applied as an anti-breast cancer agent and had dual targeting properties against EGFR and HER2.
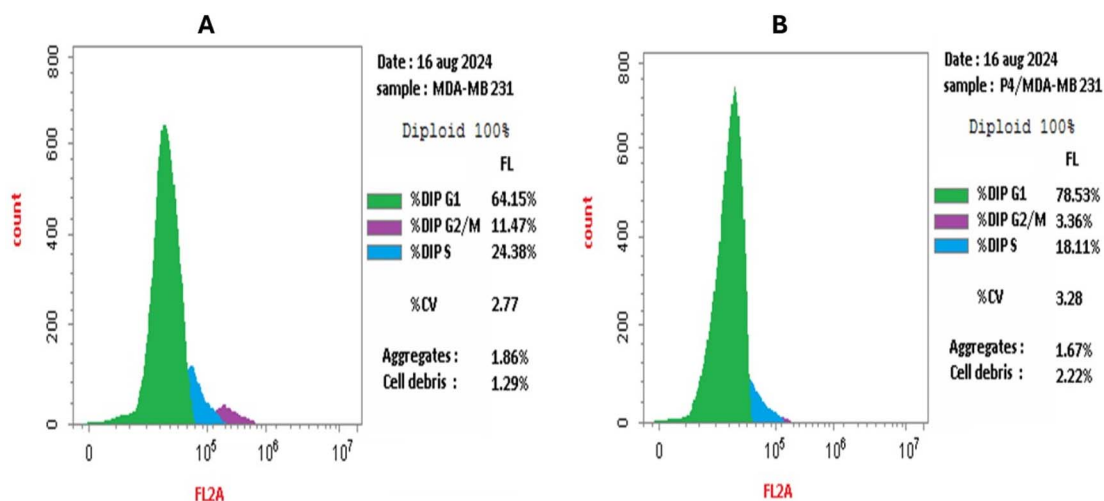
3.2.5. Cell cycle analysis and apoptosis. Compound **5d** was evaluated for its impact on the cell cycle of MDA-MB 231 cancer cells.[31] After 24 hours of treatment at 25 μM, a significant pre-G1 peak was observed, indicating apoptosis. Cell cycle analysis revealed a substantial G1 phase arrest, suggesting a potential mechanism for the observed cell death. Analysis of the results (Table 4 and Fig. 4) showed that compound **5d** can induce a percentage of pre-G1 apoptosis on MDA-MB 231 by 78.53% after 24 h incubation. Annexin V/PI staining confirmed compound **5d**′s ability to induce apoptosis, with early apoptosis being more pronounced than late apoptosis with necrosis percent 5.28 (Table 5 and Fig. 5). On the other hand, compound **5d** was able to enhance early apoptosis more than late apoptosis by 5-fold.

3.3. Molecular docking study and molecular dynamics simulation

To gain insight into the potential interaction mechanisms of both **4n** and **5d** with EGFR or HER2, we modeled the structures of these compounds and then used Autodock Vina[37] to dock them into the active sites of the kinase domains of each receptor (PDB IDs 1M17 and 3PP0, respectively).[38] We used PyMOL software[39] to edit and visualize the resulting binding poses. In

Fig. 4 Cell cycle analysis of MDA-MB 231 cells treated with (A) vehicle (control), (B) compound **5d** (0.250 μM).
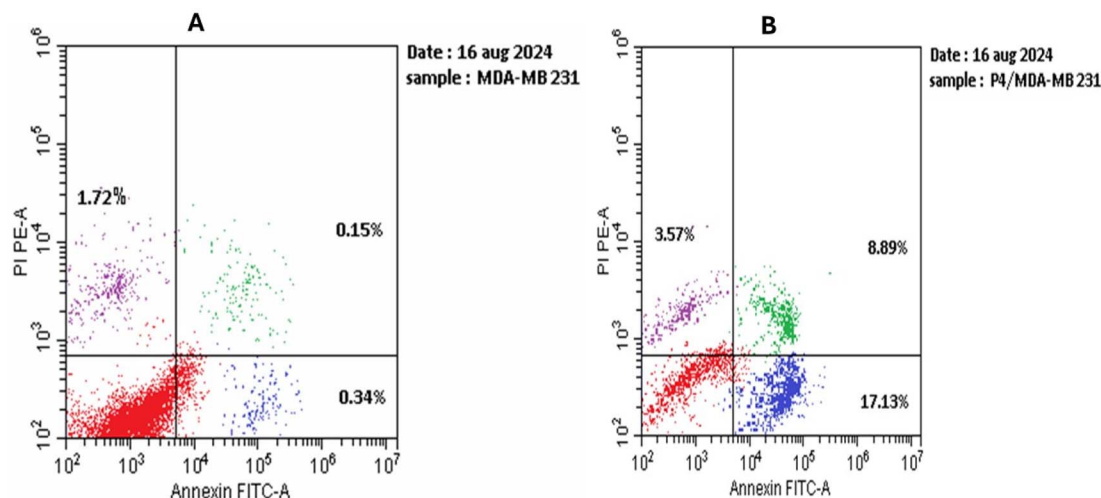
Fig. 5 Detection of apoptosis in MDA–MB 231 cells. (A): vehicle control, (B) compound **5d** (0.250 µM).

our docking experiments, we used the modeled structures of both **5d** enantiomers (*R* and *S*) as a racemic combination. The docking scores and binding patterns of compound **4n** and the *R* enantiomer of **5d** were similar in the active site of the EGFR kinase domain (−10.94 and −10.16 kcal mol^{-1}, respectively). However, the docking scores of **4n** were higher than those of **5d** (*i.e.*, the *R* enantiomer) in the active site of the HER2 kinase domain (−12.34 and −9.11 kcal mol^{-1}, respectively). The **5d** *S* enantiomer exhibited significantly worse compatibility inside the active regions of both kinase domains, with docking scores of −7.3 and −7.1 kcal mol^{-1} for EGFR and HER2, respectively.

To better understand how each compound interacts with the active parts of the kinase domains of both receptors, we simulated their docking positions for 200 ns[34–36,40,41]. After that, we looked at each MD trajectory to find the chemical's main

binding conformation, its RMSD profile, and its absolute binding free energies (ΔG_{Bind}). Fig. 6A–C illustrate that the MD simulation-derived predominant binding modes of compounds **4n** and **5d** (*R* enantiomer) when they were combined with the co-crystallized inhibitor inside the EGFR kinase domain. These interactions revealed several important details about their binding affinities and how they work.

For compound **4n**, we detected a stable hydrogen bond with the THR-766 residue (89% of simulation duration), which acts as an anchoring point within the binding pocket. Hydrophobic residues, such as LEU-820, LEU-834, VAL-702, and PHE-699, enhance the stability of **4n** *via* van der Waals interactions. The closeness of extra residues like ASP-831 and MET-742 supports the idea that they bind through non-polar interactions even more. The aromatic rings of compound **4n** indicate potential pi–
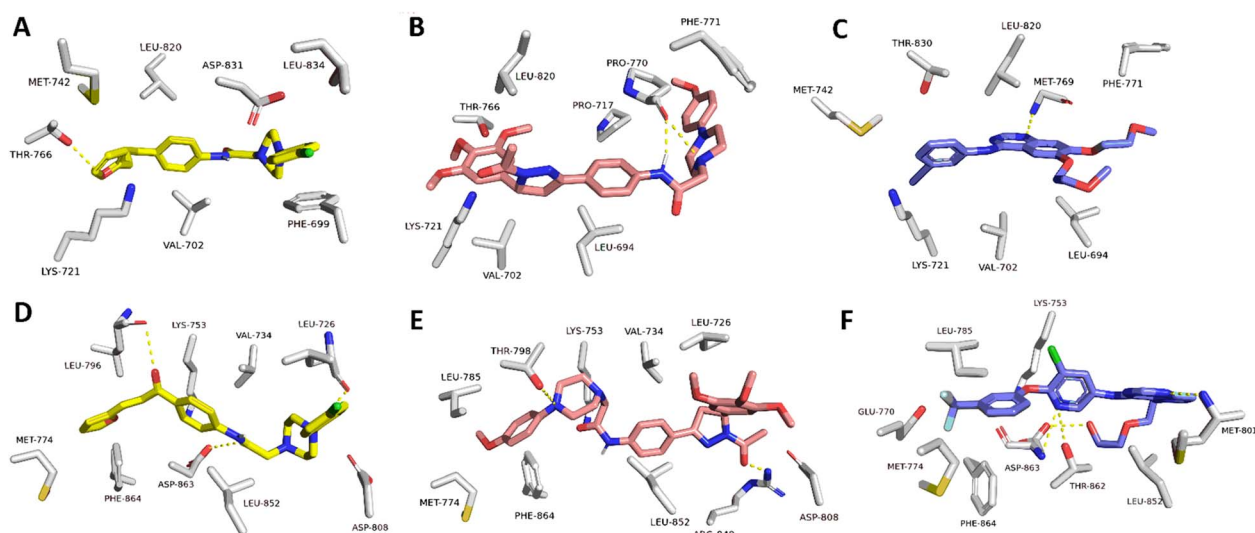

Fig. 6 Dynamic binding modes of **4n** (yellow structure), **5d** (*R* enantiomer; brick red structure), and the co-crystallized inhibitors (blue structures) inside the active sites of kinase domains of both EGFR ((A)–(C), respectively; PDB ID 1M17) and HER2 ((D)–(F), respectively; PDB ID 3PP0). The depicted binding poses were retrieved from the MD simulation trajectories as the most populated binding pose.

pi stacking interactions with PHE-699, which occurred for 57% of the simulation duration, thereby increasing its binding affinity. Furthermore, the terminal electron-deficient chlorophenyl ring engaged in stable π-anion interactions with the negatively charged residue ASP-831 (85% of the simulation duration).

Regarding **5d** (*R* configuration), its structure exhibited a distinct binding profile, characterized by a stable hydrogen bond with PRO-770 (76% of simulation time), which helps establish its orientation within the kinase pocket. Hydrophobic interactions involving residues such as LEU-820, VAL-702, and LEU-694 provide additional stabilization. The presence of PHE-771 PRO-717 and PRO-770 in the vicinity suggests further HER hydrophobic interactions, strengthening the binding of compound **5d**. Moreover, the *p*-methoxy aromatic ring of **5d** potentially engages in T-shaped pi–pi stacking with PHE-771 (55% of simulation time). In comparison, the electron-rich tri-methoxy one formed a stable π-cation interaction with LYS-721 (89% of simulation time), enhancing its affinity for the kinase domain.

The dynamic binding modes of both **4n** and **5d** (*R* enantiomer) shared a common interaction with the co-crystallized inhibitor (*i.e.*, erlotinib), particularly the hydrophobic ones with LEU-820, LEU-694, VAL-702, and PHE-771. The presence of aromatic rings in all three molecules also allows for potential pi–pi stacking with pivotal residues like PHE-699 and PHE-771, contributing to their binding affinity and specificity. These interactions highlight the compounds' capabilities to fit within the hydrophobic pocket of the kinase domain, thereby informing their potential as EGFR inhibitors.

These binding behaviors of both **4n** and **5d** (*R* enantiomer) were translated into steady RMSD profiles throughout MD simulations comparable to that of the co-crystalized inhibitor (average RMSD = 2.44 Å; Fig. 7A). Hence, their estimated ΔG_{Bind} values were convergent (−9.24, −9.48, −9.39, respectively).

As shown in Fig. 7A, compound **4n** demonstrates the highest structural stability within the binding pocket, as reflected by its consistently lower RMSD values, ranging between 1.0 and 3.0 Å. Its RMSD profile stabilizes around 2.0 Å relatively early in the simulation (after approximately 20 ns) and exhibits minimal fluctuations afterward. This behavior suggests compound **4n** forms a rigid and stable complex with the EGFR kinase domain, potentially indicating a strong binding affinity and specificity.

In contrast, compound **5d** (*R* enantiomer) displays the highest fluctuation in its RMSD values, oscillating between 1.5 and 4.0 Å throughout the simulation period. This high level of variability suggests that compound **5d** undergoes significant conformational changes, indicating a more flexible or adaptable binding mode within the kinase pocket. Such flexibility may imply weaker interactions with EGFR, potentially resulting in lower binding affinity or specificity than compound **4n** and the co-crystallized inhibitor.

The co-crystallized inhibitor shows intermediate behavior, with RMSD values fluctuating between 1.5 and 3.5 Å. While the inhibitor exhibits more flexibility than compound **4n**, it is notably more stable than compound **5d**. The RMSD pattern suggests that the co-crystallized inhibitor maintains a relatively stable interaction within the EGFR kinase domain while allowing some conformational flexibility. This balance between
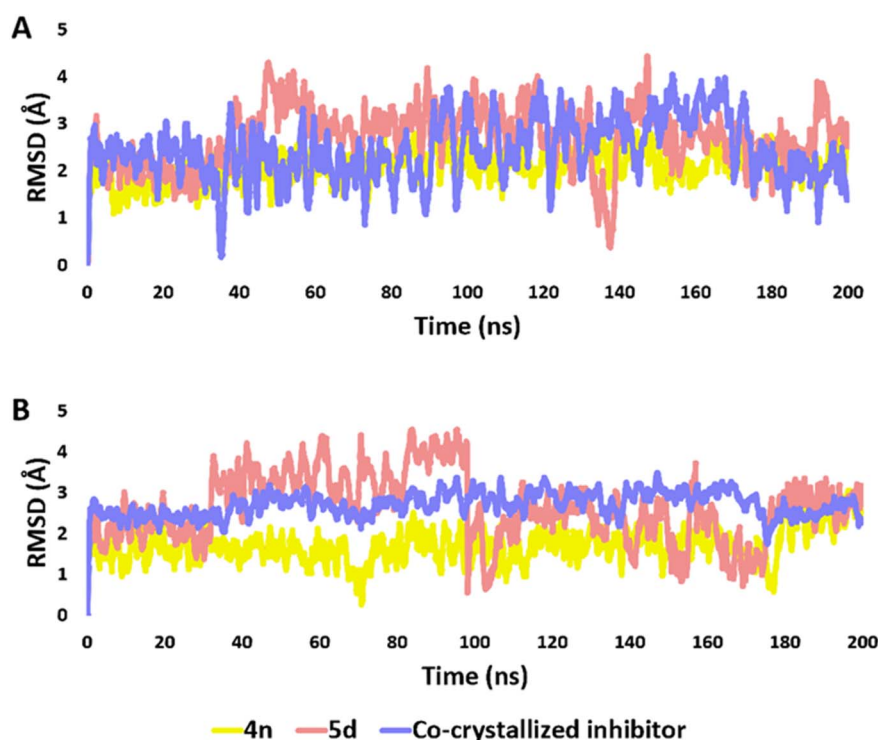

Fig. 7 RMSD profiles of **4n**, **5d**, and the co-crystallized inhibitors inside the active sites of kinase domains of both EGFR (A) and HER2 (B) throughout 200 ns MD simulation.

stability and flexibility may reflect the inhibitor's ability to achieve effective binding while accommodating necessary structural adjustments during the simulation.

Regarding HER2's kinase domain, Fig. 6D–F (representing the most populated poses of **4n** and **5d** alongside the co-crystallized inhibitor) demonstrated that both **4n** and **5d** (*R* enantiomer) exhibited comparable interactions inside the active site of HER2's kinase domain that were also concurrent to that of the co-crystallized inhibitor. **4n** forms three stable hydrogen bonds with the main chain of LEU-726 and LEU-796, alongside the side chain of ASP-863 (78%, 75%, and 71% of the simulation time, respectively) that serve as key anchoring interactions in the kinase domain's active site. The compound's proximity to ASP-808 suggests the presence of π-anion interaction (88% of simulation time) with the terminal electron deficient chlorophenyl ring that further stabilizes the binding conformation. Hydrophobic residues, including LEU-726, LEU-796, VAL-734, and LEU-852, likely engage in van der Waals interactions with the hydrophobic regions of compound **4n**, reinforcing its affinity for the binding site. Furthermore, MET-774 and PHE-864 stabilize the compound within the kinase domain through hydrophobic contacts.

For compound **5d** (*R* enantiomer), the docking pose reveals stable hydrogen bonds with LYS-753, THR-798, and ARG-849 (66%, 53%, and 61% of simulation time, respectively), facilitating its precise orientation and interaction within the binding pocket. This hydrogen-bonding network, particularly with LYS-753, mirrors typical interactions observed in effective HER2 inhibitors.[38] The surrounding hydrophobic environment, composed of residues such as LEU-726, VAL-734, LEU-785, and LEU-852, plays a crucial role in stabilizing compound **5d**. The involvement of residues like MET-774 and PHE-864 provides further hydrophobic contacts, contributing to the compound's overall stability. The aromatic rings of compound **5d** also likely engage in T-shaped pi–pi stacking interactions with PHE-864, reinforcing its binding affinity within the HER2 kinase domain.

The co-crystallized inhibitor demonstrates a well-defined binding profile characterized by a network of hydrogen bonds involving ASP-863, THR-862, and LYS-753. These interactions are vital for the inhibitor's specificity and robust binding within the kinase domain. The hydrophobic surroundings, including LEU-726, LEU-852, and MET-801, enhance the inhibitor's stability through van der Waals interactions. Potential pi–pi stacking with PHE-864 further strengthens the inhibitor's binding affinity.

Collectively, these results illustrate that compounds **4n** and **5d** (*R* enantiomer) share key binding features with the co-crystallized inhibitor, such as hydrogen bonding, hydrophobic contacts, and pi–pi stacking interactions. These compounds' ability to occupy and stabilize within the HER2 kinase pocket underscores their potential as HER2 inhibitors, providing valuable insights for further optimization and development.

The RMSD profiles and ΔG_{Bind} values of both compounds were also convergent and comparable to those of the co-crystallized inhibitor, indicating stable binding modes (average RMSD = 2.88 Å; ΔG_{Bind} values = −9.22, −8.29, −9.89 kcal mol^{-1}, respectively; Fig. 7B).

Among the three compounds, **4n** displays the lowest and most consistent RMSD values, predominantly fluctuating between 1.0 and 2.5 Å throughout the 200 ns simulation. This low range and steady fluctuation indicate that compound **4n** maintains a rigid and stable interaction within the HER2 binding pocket. The minimal structural deviations from the initial conformation suggest that **4n** fits snugly within the binding site, potentially reflecting a strong binding affinity and a well-defined interaction with the kinase domain (Fig. 7B).

In contrast, **5d** (*R* enantiomer) shows higher RMSD fluctuations, ranging between 1.5 and 4.0 Å, indicating a more dynamic interaction with the HER2 kinase domain. These larger oscillations suggest that compound **5d** undergoes notable conformational adjustments throughout the simulation, implying a more flexible binding mode. Such flexibility might indicate weaker binding affinity or a less optimized fit within the binding pocket, as the compound seems to require continuous adjustments to accommodate its position (Fig. 7B).

The co-crystallized inhibitor exhibits intermediate RMSD values, generally fluctuating between 2.0 and 3.5 Å. While it displays more variability than compound **4n**, it remains more stable than compound **5d**. This intermediate pattern suggests that the co-crystallized inhibitor maintains a relatively stable conformation within the kinase domain, similar to compound **4n**, but with a degree of flexibility that could be advantageous for effective binding. The balance of moderate flexibility and overall stability aligns with its role as a known inhibitor of HER2.

4. Conclusion

We synthesized a novel series of two scaffold compounds, chalcone/phenylpiperazine scaffold **4a–n** and pyrazoline/phenylpiperazine scaffold **5a–n** and evaluated their antiproliferative activity against EGFR and HER2. The results indicated that the compounds of scaffold B, **5a–n**, exhibited more potency than those of scaffold A, **4a–n**. Compounds **4n**, **5d**, and **5g** exhibited the highest efficacy among all evaluated compounds against a panel of four cancer cell lines. These three derivatives were subsequently examined for mechanistic analysis against EGFR-TK and HER-2. Compound **5d** was identified as an efficient antiproliferative agent that acts as a dual EGFR/HER2 inhibitor and demonstrated cell cycle arrest at the pre-G1 phase. The docking investigation and molecular dynamics simulation indicated that compounds **4n** and **5d** (*R* enantiomer) exhibit essential binding characteristics with the co-crystallized inhibitor, including hydrogen bonding, hydrophobic interactions, and pi–pi stacking interactions. All *in vitro* experiments demonstrated that **5d** is a promising lead compound that requires more structural modification to give a more potent derivative.

Data availability

Data will be available upon request from the authors.

Author contributions

H. M. Hafez: formal analysis, methodology, software, writing–original draft. B. A. M. Said: investigation, validation, visualization, writing–original draft. A. M. Sayed: methodology, writing–original draft. E. Alatwi: writing–original draft. SB: investigation, validation, visualization, writing–review and editing. BY: conceptualization, data duration, formal analysis, investigation, methodology, resources, software, supervision, validation, visualization, writing–original draft, writing–review and editing. H. A. M. El-Sherief: methodology, resources, software, writing–original draft, writing–review and editing.

Conflicts of interest

The authors declare that they have no known competing financial interests or personal relationships that could have appeared to influence the work reported in this paper.

Acknowledgements

References

1 T. Kovacs, F. Zakany and P. Nagy, *Cancers*, 2022, **14**, 944.
2 D. Kumar and M. I. Hassan, in *Receptor Tyrosine Kinases in Neurodegenerative and Psychiatric Disorders*, Elsevier, 2023, pp. 245–276.
3 Z. Batool, A. Azfal, L. Liaquat, S. Sadir, R. Nisar, A. Inamullah, A. U. F. Ghalib and S. Haider, in *Receptor Tyrosine Kinases in Neurodegenerative and Psychiatric Disorders*, Elsevier, 2023, pp. 117–185.
4 C. B. Pulivarthi, S. S. Choubey, S. K. Pandey, A. S. Gautam and R. K. Singh, *Receptor Tyrosine Kinases in Neurodegenerative and Psychiatric Disorders*, 2023, pp. 45–77.
5 Z. Batool, A. Azfal, L. Liaquat, S. Sadir, R. Nisar, A. Inamullah, A. U. F. Ghalib and S. Haider, in *Receptor Tyrosine Kinases in Neurodegenerative and Psychiatric Disorders*, Elsevier, 2023, pp. 117–185.
6 L. H. Al-Wahaibi, A. M. Elshamsy, T. F. Ali, B. G. Youssif, S. Bräse, M. Abdel-Aziz and N. A. El-Koussi, *ACS Omega*, 2024, **9**, 34358–34369.
7 L. H. Al-Wahaibi, B. G. Youssif, H. A. Abou-Zied, S. Bräse, A. B. Brown, H. N. Tawfeek and E. M. El-Sheref, *RSC Med. Chem.*, 2024, **15**, 2538–2552.
8 J. Yoon and D.-Y. Oh, *Nat. Rev. Clin. Oncol.*, 2024, 1–26.
9 D. Gandhi, A. Sethiya, N. Sahiba, D. K. Jangid and S. Agarwal, in *Nanocatalysis*, CRC Press, 2022, pp. 219–243.
10 D. O. Ozgun, H. I. Gul, C. Yamali, H. Sakagami, I. Gulcin, M. Sukuroglu and C. T. Supuran, *Bioorg. Chem.*, 2019, **84**, 511–517.
11 M. Karabacak, M. D. Altıntop, H. İ. Çiftçi, R. Koga, M. Otsuka, M. Fujita and A. Özdemir, *Molecules*, 2015, **20**, 19066–19084.
12 L. H. Al-Wahaibi, H. A. Abou-Zied, E. A. Beshr, B. G. Youssif, A. M. Hayallah and M. Abdel-Aziz, *Int. J. Mol. Sci.*, 2023, **24**, 9104.
13 L. H. Al-Wahaibi, H. A. Abou-Zied, M. Hisham, E. A. Beshr, B. G. Youssif, S. Bräse, A. M. Hayallah and M. Abdel-Aziz, *Molecules*, 2023, **28**, 6586.
14 P.-C. Lv, H.-Q. Li, J. Sun, Y. Zhou and H.-L. Zhu, *Bioorg. Med. Chem.*, 2010, **18**, 4606–4614.
15 M. Al-Anazi, M. Khairuddean, B. O. Al-Najjar, M. M. Alidmat, N. N. S. N. M. Kamal and M. Muhamad, *Arab. J. Chem.*, 2022, **15**, 103864.
16 B. Sever, M. D. Altıntop, M. O. Radwan, A. Özdemir, M. Otsuka, M. Fujita and H. I. Ciftci, *Eur. J. Med. Chem.*, 2019, **182**, 111648.
17 H. A. Jasim, L. Nahar, M. A. Jasim, S. A. Moore, K. J. Ritchie and S. D. Sarker, *Biomolecules*, 2021, **11**, 1203.
18 A. Rammohan, J. S. Reddy, G. Sravya, C. N. Rao and G. V. Zyryanov, *Environ. Chem. Lett.*, 2020, **18**, 433–458.
19 M. Hisham, H. A. Hassan, H. A. Gomaa, B. G. Youssif, A. M. Hayalah and M. Abdel-Aziz, *Anti-Cancer Agents Med. Chem.*, 2023, **23**, 1932–1943.
20 M. Hisham, H. A. Hassan, H. A. Gomaa, B. G. Youssif, A. M. Hayallah and M. Abdel-Aziz, *J. Mol. Struct.*, 2022, **1254**, 132422.
21 J. Xiao, M. Gao, Q. Diao and F. Gao, *Curr. Top. Med. Chem.*, 2021, **21**, 348–362.
22 F. F. Leite, N. F. de Sousa, B. H. M. de Oliveira, G. D. Duarte, M. D. L. Ferreira, M. T. Scotti, J. M. B. Filho, L. C. Rodrigues, R. O. de Moura and F. J. B. Mendonça-Junior, *Molecules*, 2023, **28**, 4009.
23 P. Kumar, R. Singh, D. Sharma, Q. P. Hassan, B. Gopu and J. M. H. Anal, *Bioorg. Med. Chem. Lett.*, 2024, **107**, 129795.
24 A. M. Mohassab, H. A. Hassan, D. Abdelhamid, A. M. Gouda, B. G. Youssif, H. Tateishi, M. Fujita, M. Otsuka and M. Abdel-Aziz, *Bioorg. Chem.*, 2021, **106**, 104510.
25 H. A. Abou-Zied, E. A. Beshr, H. A. Gomaa, Y. A. Mostafa, B. G. Youssif, A. M. Hayallah and M. Abdel-Aziz, *Arch. Pharm.*, 2023, **356**, 2200464.
26 L. H. Al-Wahaibi, E. M. El-Sheref, A. A. Hassan, S. Bräse, M. Nieger, B. G. Youssif, M. A. Ibrahim and H. N. Tawfeek, *Pharmaceuticals*, 2023, **16**, 1014.
27 L. H. Al-Wahaibi, M. A. Mahmoud, Y. A. Mostafa, A. E. Raslan and B. G. Youssif, *J. Enzyme Inhib. Med. Chem.*, 2023, **38**, 376–386.
28 L. H. Al-Wahaibi, A. F. Mohammed, F. E.-Z. S. A. Rahman, M. H. Abdelrahman, X. Gu, L. Trembleau and B. G. Youssif, *J. Enzym. Inhib. Med. Chem.*, 2023, **38**, 2218602.
29 R. A. Mekheimer, S. M. Allam, M. A. Al-Sheikh, M. S. Moustafa, S. M. Al-Mousawi, Y. A. Mostafa, B. G. Youssif, H. A. Gomaa, A. M. Hayallah and M. Abdelaziz, *Bioorg. Chem.*, 2022, **121**, 105693.
30 S. E. Wang, A. Narasanna, M. Perez-Torres, B. Xiang, F. Y. Wu, S. Yang, G. Carpenter, A. F. Gazdar, S. K. Muthuswamy and C. L. Arteaga, *Cancer Cell*, 2006, **10**, 25–38.
31 P. Smolewski, E. Bedner, L. Du, T. C. Hsieh, J. M. Wu, D. J. Phelps and Z. Darzynkiewicz, *Cytometry: The Journal of*

the *International Society for Analytical Cytology*, 2001, **44**, 73–82.

32 E. Brahmana, J. Kaban, G. Haro and M. Ginting, *Rasayan J. Chem.*, 2022, **15**, 3–11.

33 M. A. Mahmoud, A. F. Mohammed, O. I. Salem, H. A. Gomaa and B. G. Youssif, *Arch. Pharm.*, 2022, **355**, 2200009.

34 M. S. Mohamed, H. A. Elsherief, H. M. Hafez, O. A. Alsaidan, S. I. Alzarea and A. M. AboulMagd, *Mol. Diversity*, 2023, **27**, 2133–2146.

35 M. Johnson, B. Younglove, L. Lee, R. LeBlanc, H. Holt Jr, P. Hills, H. Mackay, T. Brown, S. L. Mooberry and M. Lee, *Bioorg. Med. Chem. Lett*, 2007, **17**, 5897–5901.

36 F. F. Hagar, S. H. Abbas, D. Abdelhamid, H. A. Gomaa, B. G. Youssif and M. Abdel-Aziz, *Arch. Pharm.*, 2023, **356**, 2200357.

37 J. Eberhardt, D. Santos-Martins, A. F. Tillack and S. Forli, *J. Chem. Inf. Model.*, 2021, **61**, 3891–3898.

38 K. Aertgeerts, R. Skene, J. Yano, B.-C. Sang, H. Zou, G. Snell, A. Jennings, K. Iwamoto, N. Habuka and A. Hirokawa, *J. Biol. Chem.*, 2011, **286**, 18756–18765.

39 S. Yuan, H. S. Chan and Z. Hu, *Wiley Interdiscip. Rev.: Comput. Mol. Sci.*, 2017, **7**, e1298.

40 J. V. Ribeiro, R. C. Bernardi, T. Rudack, K. Schulten and E. Tajkhorshid, *Biophys. J.*, 2018, **114**, 673a–674a.

41 W. Humphrey, A. Dalke and K. Schulten, *J. Mol. Graph.*, 1996, **14**, 33–38.